iScience

CellPress
OPEN ACCESS

Article

Gene repression through epigenetic modulation by PPARA enhances hepatocellular proliferation

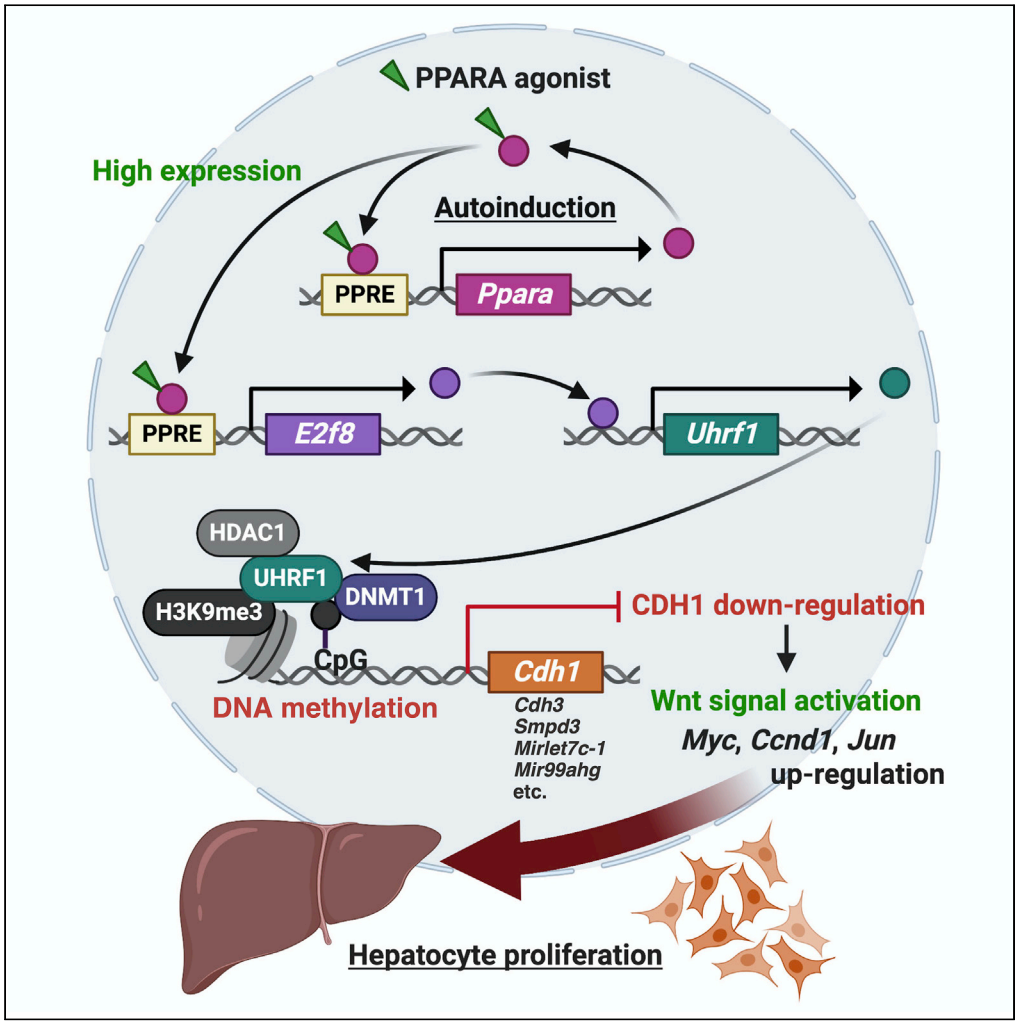

Daisuke Aibara, Shogo Takahashi, Tomoki Yagai, ..., Moshe Levi, Kimihiko Matsusue, Frank J. Gonzalez

shogo.takahashi@nih.gov (S.T.)
gonzalef@mail.nih.gov (F.J.G.)

Highlights

PPARA activation induces the UHRF1 expression via novel PPARA target gene *E2f8*

Induction of UHRF1 by PPARA activation represses *Cdh1* gene marked with H3K9me3

CDH1 suppresses hepatocyte proliferation after PPARA activation

Autoinduction of PPARA by agonist enhances cell proliferation via E2F8-UHRF1-CDH1

Aibara et al., iScience *25*, 104196
May 20, 2022
https://doi.org/10.1016/j.isci.2022.104196

iScience

CellPress
OPEN ACCESS

Article

Gene repression through epigenetic modulation by PPARA enhances hepatocellular proliferation

Daisuke Aibara,[1,2] Shogo Takahashi,[1,3,*] Tomoki Yagai,[1] Donghwan Kim,[1] Chad N. Brocker,[1] Moshe Levi,[3] Kimihiko Matsusue,[2] and Frank J. Gonzalez[1,4,*]

SUMMARY

Peroxisome proliferator-activated receptor α (PPARA) is a key mediator of lipid metabolism and inflammation. Activation of PPARA in rodents causes hepatocyte proliferation, but the underlying mechanism is poorly understood. This study focused on genes repressed by PPARA and analyzed the mechanism by which PPARA promotes hepatocyte proliferation in mice. Activation of PPARA by agonist treatment was autoregulated, and induced expression of the epigenetic regulator UHRF1 via activation of the newly described PPARA target gene *E2f8*, which, in turn, regulates *Uhrf1*. UHRF1 strongly repressed the expression of CDH1 via methylation of the *Cdh1* promoter marked with H3K9me3. Repression of CDH1 by PPARA activation was reversed by PPARA deficiency or knockdown of E2F8 or UHRF1. Furthermore, a forced expression of CDH1 inhibited expression of the Wnt signaling target genes such as *Myc* after PPARA activation, and suppressed hepatocyte hyperproliferation. These results demonstrate that the PPARA-E2F8-UHRF1-CDH1 axis causes epigenetic regulation of hepatocyte proliferation.

INTRODUCTION

Peroxisome proliferator-activated receptor α (PPARA) is a ligand-activated nuclear receptor abundantly expressed in hepatocytes and an important mediator of lipid metabolism and inflammation (Brocker et al., 2020; Dubois et al., 2017; Kamata et al., 2020). Chronic activation of PPARA causes hepatocellular proliferation and increases the incidence of hepatocellular carcinoma (HCC) in rodents (Brocker et al., 2017; Kim et al., 2019; Morimura et al., 2006). The myelocytomatosis oncogene (*Myc*) contributes to PPARA agonist-induced hepatocyte proliferation. Hepatocyte proliferation induced by MYC was verified in liver-specific MYC-deficient mice treated with PPARA agonists. Interestingly, PPARA agonist-induced hepatocyte proliferation was not fully protected by liver-specific deficiency of MYC (Qu et al., 2014). These results indicate that PPARA may contribute to hepatocyte proliferation by regulating the expression of *Myc* and other genes involved in cell proliferation.

The regulation of gene expression by PPARA is through a standard ligand-dependent mechanism used by Type 2 nuclear receptors. PPARA forms a heterodimer with the retinoid X receptor α (RXRA), and when an agonist ligand such as pirinixic acid (Wy14,643) or synthetic fibric acid derivatives (e.g., fenofibrate) binds to PPARA, co-repressors are released and co-activators are recruited upon binding to the PPARA response element (PPRE) of the target gene-enhancer/promoter region (Berger and Moller, 2002; Kang and Fan, 2020; Pawlak et al., 2015). The PPARA complex bound to the PPRE positively regulates the expression of target genes (Berger and Moller, 2002; Penvose et al., 2019). Whereas activated PPARA positively regulates target gene expression, some studies have shown that PPARA can negatively regulate gene expression (Pawlak et al., 2015). However, the mechanism of ligand-dependent negative regulation of gene expression by nuclear receptors, including PPARA, that is, gene repression/gene silencing, is mechanistically poorly understood.

Repression of E-cadherin/cadherin 1 (*Cdh1*) causes cell proliferation (Shang et al., 2017). In the current study, *Cdh1* was identified as a gene strongly repressed by PPARA, and the mechanism by which PPARA controls cell proliferation through CDH1 repression was analyzed in mouse livers. The current study

[1]Laboratory of Metabolism, Center for Cancer Research, National Cancer Institute, National Institutes of Health, Bethesda, MD 20892, USA

[2]Faculty of Pharmaceutical Science, Fukuoka University, 8-19-1 Nanakuma, Jonan-ku, Fukuoka 814-0180, Japan

[3]Department of Biochemistry and Molecular and Cellular Biology, Georgetown University, Washington, DC 20057, USA

[4]Lead contact

*Correspondence: shogo.takahashi@nih.gov (S.T.), gonzalef@mail.nih.gov (F.J.G.)

https://doi.org/10.1016/j.isci.2022.104196

revealed the existence of a novel PPARA autoinduction pathway. In addition, PPARA was found to indirectly induce the epigenetic regulator ubiquitin-like, containing PHD and RING finger domains 1 (UHRF1) via a newly described PPARA target gene encoding E2F transcription factor 8 (E2F8). UHRF1 induced by activated PPARA represses the expression of CDH1 via methylation of the *Cdh1* promoter marked with histone H3 containing the trimethylated lysine 9 (H3K9me3); knockdown of E2F8 or UHRF1-reversed CDH1 repression. Furthermore, forced expression of CDH1 repressed PPARA agonist-induced hepatocyte proliferation by suppressing expression of the Wnt signaling target genes *Myc*, cyclin D1 (*Ccnd1*), and jun proto-oncogene (*Jun*). These results indicate that PPARA autoinduction enhances hepatocyte proliferation via the E2F8-UHRF1-CDH1-Wnt signaling axis. In addition, this study provided mechanism by which nuclear receptors repress gene expression.

RESULTS

Expression of CDH1 is strongly repressed by ligand-activated PPARA

Agonist activation of mouse PPARA promotes hepatocyte proliferation (Peters et al., 2012). However, the mechanism of hepatocyte proliferation by PPARA is poorly understood (Kim et al., 2019). Epigenetic silencing of certain tumor suppressor genes (TSGs) cause cell proliferation. To investigate the major TSGs that are repressed by activated PPARA, RNA sequencing (RNA-seq) was performed on livers of *Ppara* wild-type ($Ppara^{+/+}$) mice treated for 48 h with two PPARA agonists used in previous studies (Kim et al., 2019; Morimura et al., 2006), Wy14,643 and fenofibrate; *Ppara*-null ($Ppara^{-/-}$) mice were used as a negative control. A mix of total RNA from three to five mice was used per RNA-seq experiment and repeated three times in each group (n = 10–15 mice per group). Both Wy14,643 and fenofibrate treatment induced expression of 370 genes and repressed expression of 248 genes, at a fold-change > 3 and a false discovery rate (FDR) < 0.05, in $Ppara^{+/+}$ mouse livers (Figures 1A, S1, and Table S1). The 370 genes induced by both Wy14,643 and fenofibrate treatment included typical PPARA target genes such as cytochrome P450 family four subfamily A polypeptide 10 (*Cyp4a10*), acyl-coenzyme A oxidase 1 (*Acox1*), acyl-CoA thioesterase 1 and 2 (*Acot1* and *Acot2*) (Table S1). In addition, Wy14,643 treatment yielded more potent PPARA target gene activation than fenofibrate treatment (Figures 1A, S1, and Table S1). Therefore, Wy14,643 was used in the present study.

Haploinsufficient TSGs repressed by PPARA agonists were also investigated by the DAVID-GO (https://david.ncifcrf.gov/) and previous lists (Inoue and Fry, 2017; Payne and Kemp, 2005). *Cdh1* was identified as a gene that was significantly repressed by activated PPARA (Figure 1B). To confirm the results of RNA sequencing, qPCR (n = 4 mice per group) and western blotting (n = 3 mice per group) were performed using randomly selected mouse livers. Quantitative analysis showed that the expression of *Cdh1* mRNA and CDH1 in the $Ppara^{+/+}$ mouse livers was significantly repressed by Wy14,643 or fenofibrate treatment by more than 50% (Figures 1C–1E). On the other hand, the expression of *Cdh1* mRNA and CDH1 in $Ppara^{-/-}$ mouse livers was not significantly changed by Wy14,643 and fenofibrate treatment (Figures 1C–1E). These results indicate that activated PPARA specifically represses the expression of CDH1.

The loss of CDH1 increases β-catenin nuclear signal transduction and upregulates expression of the Wnt signaling target genes *Myc*, *Ccnd1*, *Jun*, and *Axin2*. Expression of these genes is involved in cell proliferation and differentiation (Shang et al., 2017). RNA-seq was performed to investigate the global effect of PPARA repression of CDH1 on expression of the Wnt signaling target genes. The expression of the Wnt signaling target genes were weakly induced in Wy14,643-treated $Ppara^{+/+}$ mouse livers compared with the direct bonafide PPARA gene targets, *Cyp4a10*, *Acot1*, *Acot2*, and *Acox1* (Figure 1F). This result suggests that the repression of CDH1 by PPARA may activate Wnt signaling and induce the expression of its downstream genes.

Transcription regulators such as snail family zinc finger 1 and 2 (Snail1/Snail and Snail2/Slug), twist basic-helix-loop-helix transcription factor (Twist) and zinc finger E-box binding homeobox (Zeb) were reported to be involved in suppression of *Cdh1* expression (Cheng et al., 2019). Expression of *Snail1/2*, *Twist1/2*, *Zeb1/2* mRNAs were measured to investigate the mechanism of *Cdh1* repression. The levels of *Snail1*, *Twist1/2*, *Zeb1/2* mRNAs in $Ppara^{+/+}$ mouse livers were not changed by Wy14,643 treatment (Figure 1F). *Snail2* mRNA expression in $Ppara^{+/+}$ mouse livers was reduced to about 50% in all three samples by Wy14,643 treatment (Figure 1F). Snail2 is a transcription repressor of *Cdh1* (Hu et al., 2018; Villarejo et al., 2014), and suppression of Snail2 expression has been reported to increase CDH1 expression (Wang et al., 2010). However, both *Snail2* and *Cdh1* mRNA levels in $Ppara^{+/+}$ mouse livers were strongly

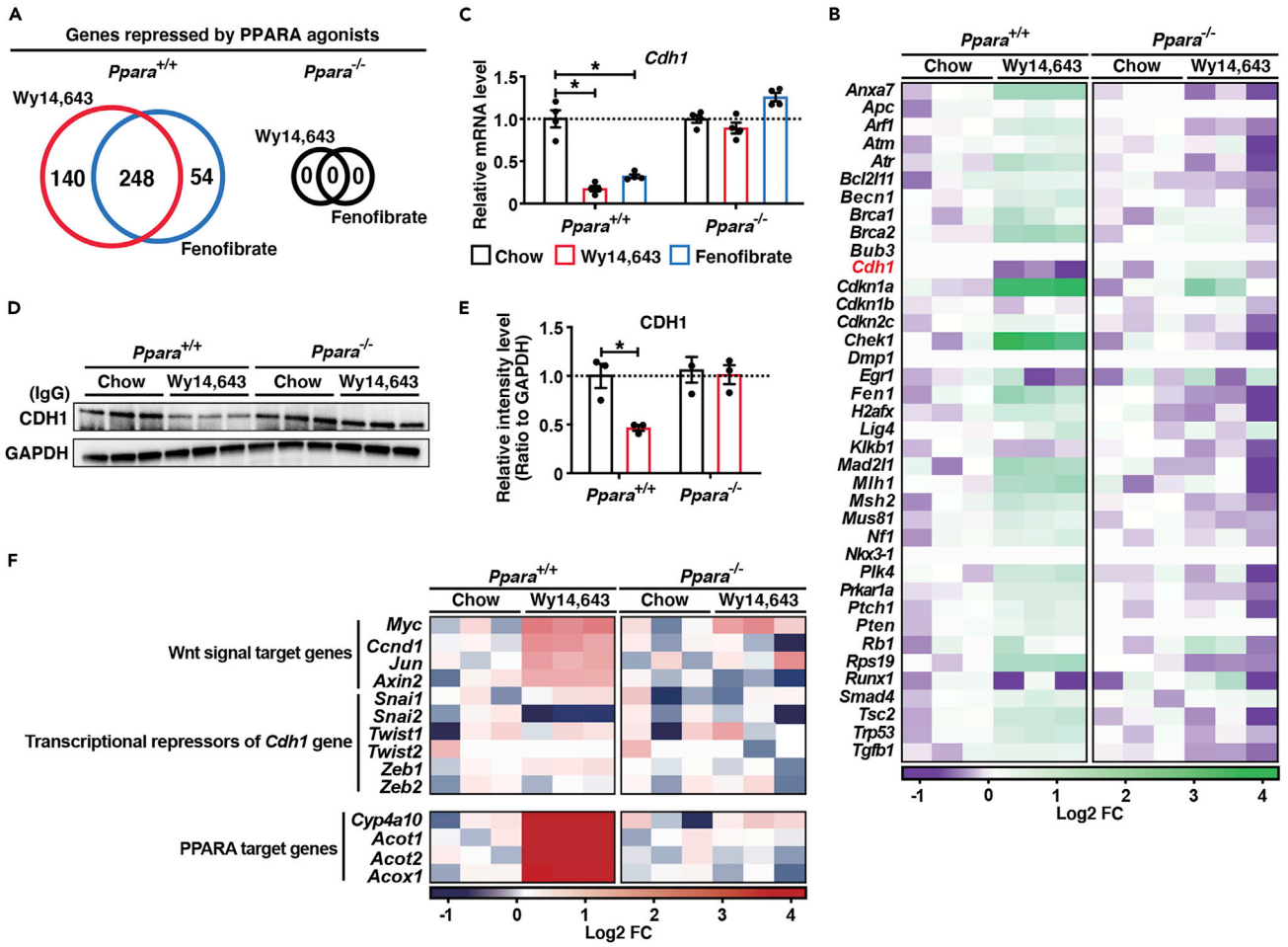

Figure 1. Ligand-activated PPARA strongly represses CDH1 expression

Ppara$^{+/+}$ and *Ppara*$^{-/-}$ mice fed either control chow diet or a diet containing 0.1% Wy14,643 or 0.5% fenofibrate for 48 h.

(A) Venn diagrams of RefSeq transcripts were repressed by Wy14,643 or fenofibrate (fold change < −3 at FDR <0.05) in *Ppara*$^{+/+}$ and *Ppara*$^{-/-}$ mouse livers, as determined by RNA-seq. n = 10–15 mice per group.

(B) Heatmap of tumor suppressor gene expression provided from RNA-seq analyses in Wy14,643-treated *Ppara*$^{+/+}$ and *Ppara*$^{-/-}$ mouse livers. n = 10–15 mice per group. Color key, Log2 fold-change (FC).

(C) RT-qPCR analysis of *Cdh1* mRNA in Wy14,643- or fenofibrate-treated *Ppara*$^{+/+}$ and *Ppara*$^{-/-}$ mouse livers. n = 4 mice per group.

(D and E) Western blot analysis (D) and the quantification (E) of CDH1 protein in Wy14,643-treated *Ppara*$^{+/+}$ and *Ppara*$^{-/-}$ mouse livers. n = 3 mice per group.

(F) Heatmap of gene expression in the CDH1-related gene and PPARA target genes provided from RNA-seq analyses of Wy14,643-treated *Ppara*$^{+/+}$ and *Ppara*$^{-/-}$ mouse livers. n = 10–15 mice per group. Color key, Log2 fold-change (FC). Each data point represents the mean ± SEM Significant differences from normal chow diet-treated each genotype mouse livers: *p < 0.001.

repressed by Wy14,643 treatment (Figures 1B, 1C, and 1F). These data suggest that repression of *Cdh1* expression by PPARA is likely caused by factors other than Snail, Slug, Twist and Zeb. Thus, activated PPARA may contribute to hepatocyte proliferation by repressing CDH1 expression and activating Wnt signaling.

Expression of the epigenetic regulator UHRF1 is indirectly induced by PPAR activation

As the repression of CDH1 by activated PPARA through factors other than Snail, Slug, Twist and Zeb was ruled out, epigenetic regulators that contribute to DNA methylation and post-translational modification of histones and contribute to gene repression (Cheng et al., 2019) were analyzed. The expression of mRNAs encoding these regulators was analyzed in Wy14,643-treated *Ppara*$^{+/+}$ and *Ppara*$^{-/-}$ mouse livers. Interestingly, most of these listed epigenetic regulators were induced in Wy14,643-treated *Ppara*$^{+/+}$ mouse livers (Figures 2A and S1A). Among the DNA methylation-related genes, the expression of *Uhrf1* mRNA in the *Ppara*$^{+/+}$ mouse livers was robustly induced by Wy14,643 treatment (Figures 2A and S1A). By quantitative

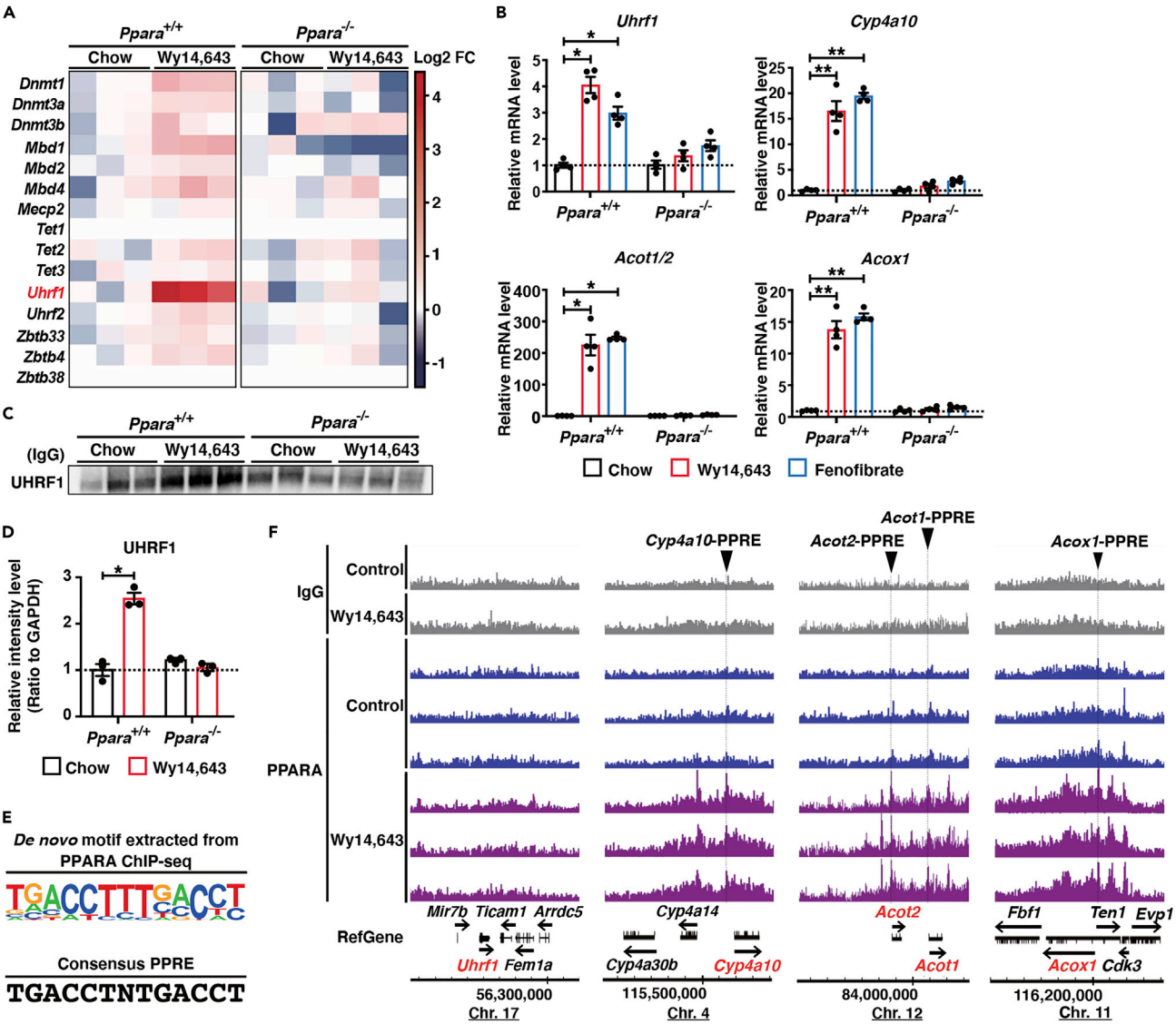

Figure 2. Activated PPARA indirectly induces expression of the epigenetic regulator UHRF1

(A) Heatmap of epigenetic regulatory genes expression provided from RNA-seq analyses in Wy14,643-treated *Ppara*$^{+/+}$ and *Ppara*$^{-/-}$ mouse livers. n = 10–15 mice per group. Mice fed either control chow diet or a diet containing 0.1% Wy14,643 for 48 h. Color key, Log2 fold-change (FC).

(B) qRT-PCR analysis of *Uhrf1*, *Cyp4a10*, *Acot1/2*, and *Acox1* mRNAs in Wy14,643- or fenofibrate-treated *Ppara*$^{+/+}$ and *Ppara*$^{-/-}$ mouse livers. n = 4 mice per group. Mice fed either control chow diet or a diet containing 0.1% Wy14,643 or 0.5% fenofibrate for 48 h.

(C and D) Western blot analysis (C) and the quantification (D) of UHRF1 protein in Wy14,643-treated *Ppara*$^{+/+}$ and *Ppara*$^{-/-}$ mouse livers. n = 3 mice per group. Mice fed either control chow diet or a diet containing 0.1% Wy14,643 or 0.5% fenofibrate for 48 h. The loading control GAPDH, detected on the same membrane, is shown in Figure 1D.

(E) *De novo* motif extracted from PPARA ChIP-seq.

(F) PPARA ChIP-seq reads the peaks of *Cyp4a10*-PPRE, *Acot1*-PPRE, *Acot2*-PPRE, and *Acox1*-PPRE from Wy14,643-treated mouse livers, but not the peaks of the *Uhrf1* gene. Mice were treated with Wy14,643 (50 mg/12 h/kg for 24 h) or vehicle by oral gavage and then administered either a normal diet or a 0.1% Wy14,643-chow diet for 24 h. n = 3 mice per group. Each data point represents the mean ± SEM Significant differences from normal chow diet-treated each genotype mouse livers: *p < 0.01; **p < 0.001.

analysis of the known PPARA target genes *Cyp4a10*, *Acot1/2*, and *Acox1* mRNAs were used as positive controls (Dongol et al., 2007; Kroetz et al., 1998; Rakhshandehroo et al., 2010). Expression of *Uhrf1*, *Cyp4a10*, *Acot1/2*, and *Acox1* mRNAs in *Ppara*$^{+/+}$ mouse livers was significantly induced by Wy14,643 and fenofibrate treatment (Figure 2B). In addition, expression of the UHRF1 protein in *Ppara*$^{+/+}$ mouse livers was

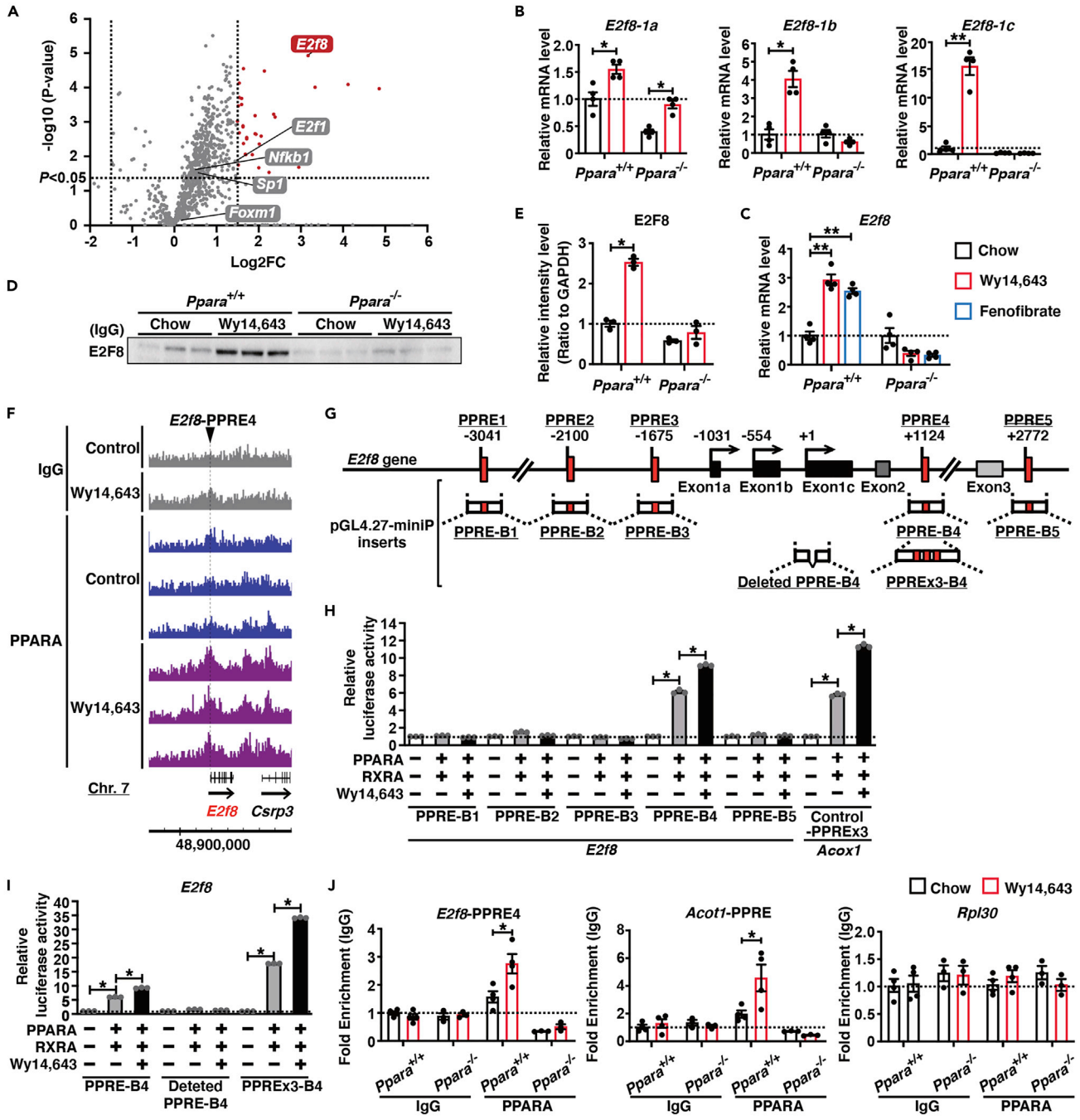

Figure 3. Activated PPARA directly induces the expression of E2F8, the regulator of *Uhrf1*

(A) Volcano plot of 1362 gene expression encoding DNA-binding transcription activity (GO:0003700) provided from RNA-seq analyses in Wy14,643-treated *Ppara*$^{+/+}$ and *Ppara*$^{-/-}$ mouse livers. Mice fed either a control chow diet or a diet containing 0.1% Wy14,643 for 48 h. n = 10–15 mice per group. The color red represents the differentially expressed genes based on $p < 0.05$ (false discovery rate = 5%; represented by black horizontal line) and 3-fold expression difference (represented by two black vertical lines).

(B and C) qRT-PCR analysis of three exon 1 variants of the *E2f8* (*E2f8-1a*, *E2f8-1b*, and *E2f8-1c*) mRNAs (B) and Total *E2f8* mRNA (C) in Wy14,643- or fenofibrate-treated *Ppara*$^{+/+}$ and *Ppara*$^{-/-}$ mouse livers. Mice fed either a control chow diet or a diet containing 0.1% Wy14,643 or 0.5% fenofibrate for 48 h. n = 4 mice per group. Significant differences from normal chow diet-treated each genotype mouse livers: *$p < 0.01$, **$p < 0.001$..

(D and E) Western blot analysis (D) and quantitation (E) of E2F8 protein in Wy14,643-treated *Ppara*$^{+/+}$ and *Ppara*$^{-/-}$ mouse livers. Mice fed either a control chow diet or a diet containing 0.1% Wy14,643 for 48 h. n = 3 mice per group. The loading control, GAPDH detected on the same membrane, is shown in Figure 1D. Significant differences from normal chow diet-treated each genotype mouse livers: *$p < 0.01$.

Figure 3. *Continued*

(F) PPARA ChIP-seq read peaks in the *E2f8* gene from Wy14,643-treated mouse livers. Mice were treated with Wy14,643 (50 mg/12 h/kg for 48 h) or vehicle by oral gavage and then administered either a normal diet or a 0.1% Wy14,643-chow diet for 24 h. $n = 3$ mice per group.

(G) Schematic representation of the positions of the putative five PPRE sequences contained in the *E2f8* gene. Reporter gene construct inserts are shown.

(H and I) Luciferase reporter assay using the PPREs of the *E2f8* gene (H) and its deleted- or amplified-PPRE4 mutant (I) confirmed functional PPRE sequence. $n = 3$ per group. Significant differences from cells without PPARA/RXRA expression plasmid or without Wy14,643: $^*p < 0.001$.

(J) PPARA ChIP-qPCR assessed *E2f8*-PPRE4, *Acot1*-PPRE, and *Rpl30* binding in liver samples from $Ppara^{+/+}$ and $Ppara^{-/-}$ mice treated with Wy14,643. Mice fed either a control chow diet or a diet containing 0.1% Wy14,643 for 48 h. $n = 3$–4 mice per group. Significant differences from normal chow diet-treated mouse livers of different genotypes: $^*p < 0.05$. Each data point represents the mean ± SEM.

significantly elevated by Wy14,643 treatment (Figures 2C and 2D). On the other hand, the levels of *Uhrf1* mRNA and UHRF1 protein in $Ppara^{-/-}$ mouse livers were not significantly changed by Wy14,643 treatment (Figures 2C–2D).

To clarify the mechanism of UHRF1 regulation by PPARA, chromatin immunoprecipitation sequencing (ChIP-seq) analysis was performed using livers from mice treated with Wy14,643. The enriched sequence in the binding peak of PPARA was motif analyzed by Homer Software (Heinz et al., 2010), and a PPRE was detected that exactly matches the consensus PPRE (Figure 2E, Dataset S1 and S2). The *Cyp4a10*, *Acot1*, *Acot2*, and *Acox1* genes were used as positive controls for PPARA binding peaks. Strong binding peaks of PPARA were observed on the PPREs of *Cyp4a10*, *Acot1*, *Acot2*, and *Acox1* in Wy14,643-treated mouse livers (Figure 2F). On the other hand, no binding peak of PPARA was observed in the *Uhrf1* promoter region of other regions of the *Uhrf1* gene (Figure 2F). These results indicate that activated PPARA indirectly induces epigenetic regulator UHRF1.

Expression of E2F8, a regulator of UHRF1, is directly induced by activated PPARA

Several transcription factors such as E2F1 and E2F8, nuclear factor of kappa light polypeptide gene enhancer in B cells 1, p105 (NFKB1), *trans*-acting transcription factor 1 (SP1) and forkhead box M1 (FOXM1) were reported to directly regulate *Uhrf1* (Ashraf et al., 2017). The expression of these transcription factor mRNAs was analyzed in Wy14,643-treated $Ppara^{+/+}$ and $Ppara^{-/-}$ mouse livers. Of the 1,362 genes encoding DNA-binding transcription activity (http://www.informatics.jax.org/, GO:0003700), the *E2f8* gene was identified as a regulator of UHRF1 that is significantly induced by PPARA (Figure 3A). In addition, E2F8 binds to the promoter region of *UHRF1* positively regulating its expression (Park et al., 2015). Therefore, regulation of the *E2f8* gene by PPARA was analyzed. The *E2f8* transcripts, *E2f8-1a*, *E2f8-1b*, and *E2f8-1c*, were reported to be exon one splice variants (Maiti et al., 2005). Quantitative analysis revealed that *E2f8* mutant mRNAs or their proteins in wild-type mouse livers were significantly induced by PPARA agonist treatment. On the other hand, these inductions were not observed in $Ppara^{-/-}$ mouse livers (Figures 3B–3E).

Five potential PPREs were identified within the PPARA ChIP-seq peaks found in closeness, proximity to the mouse *E2f8* gene by JASPAR database (https://jaspar.genereg.net/) (Figures 3F and S1B). These *E2f8*-PPREs showed greater than 69% homology with the consensus PPRE (Figure S1B). To identify which PPREs are functional, each of the five *E2f8* PPRE sites (PPRE-B1 to -B5) was inserted into pGL4.27 containing the minimal promoter, and luciferase reporter gene expression assays were performed (Figures 3G and S1C). Luciferase activity of *E2f8*-PPRE-B4 was induced approximately six-fold by PPARA/RXRA (Figure 3H). *E2f8*-PPRE-B1, B2, B3, and B5 did not respond and the PPREs do not appear to functionally bind PPARA (Figure 3H). In addition, *E2f8*-PPRE-B4 luciferase activity by PPARA/RXRA was further induced by Wy14,643 treatment similar to a reporter construct containing a PPRE repeat from the rat *Acox1* gene (Control-PPREx3) (Figure 3H). Two additional reporter constructs were created to further confirm binding of PPARA to *E2f8*-PPRE4; one contained a triple repeat of the B4 PPRE (*E2f8*-PPREx3-B4) and the other contained the same promoter insert with the *E2f8*-PPRE-B4 site removed (*E2f8*-deleted PPRE-B4) (Figures 3G and S1D). Luciferase activity induced by PPARA/RXRA was significantly amplified when the *E2f8*-PPRE-B4 was present and completely abolished when the site was deleted (Figure 3I).

Next, ChIP-quantitative real-time polymerase chain reaction (ChIP-qPCR) using primers that specifically recognize the *E2f8*-PPRE4 was used to confirm that PPARA specifically binds to the PPRE4 located in intron 2 of the *E2f8* gene. $Ppara^{-/-}$ livers were used as a negative control to test for non-specific binding. The *Acot1* gene was used as a positive control for PPARA binding enrichment, and ribosomal protein L30 (*Rpl30*) was used as a negative control. The enrichment of PPARA binding to the *E2f8* PPRE4 and *Acot1* was significantly increased in $Ppara^{+/+}$ mouse livers after Wy14,643 treatment (Figure 3J). On the other

hand, the enrichment of PPARA binding in *E2f8*-PPRE4 was not observed in *Ppara*$^{-/-}$ mouse livers (Figure 3J).

To examine whether PPARA/RXRA directly binds to *E2f8*-PPRE4, electrophoretic mobility shift assay (EMSA) using *E2f8*-PPRE4 probes was performed. PPARA/RXRA directly binds to PPRE of the rat *Acox1* as a positive control (control-PPRE) (Makia and Goldstein, 2016) and *E2f8*-PPRE4 (Figure S1F). The binding of PPARA/RXRA to *E2f8*-PPRE4 was supershifted by anti-PPARA IgG (Figure S1F). Taken together, these data suggest that PPARA positively regulates *E2f8* expression through a functional PPRE in intron 2, thereby indirectly inducing UHRF1 expression.

UHRF1 induced by PPARA activation enhances methylation of the *Cdh1* promoter marked with H3K9me3

UHRF1 has several functional domains that coordinate the DNA methylation and histone post-translational modification machinery required for epigenetic silencing of genes (Alhosin et al., 2016). UHRF1 recruits several enzymes, including DNA methyltransferase 1 (DNMT1) and histone deacetylase 1 (HDAC1), into the promoter region of target genes via H3K9me3 (Bostick et al., 2007; Karagianni et al., 2008; Kim et al., 2018; Unoki et al., 2004) as depicted in the model (Figure 4A). Therefore, the expression of UHRF1-related genes was analyzed in livers of Wy14,643-treated *Ppara*$^{+/+}$ and *Ppara*$^{-/-}$ mice. The expression of *Dnmt1* mRNA, encoding the DNA methyltransferase DNMT1, was slightly induced in Wy14,643-treated *Ppara*$^{+/+}$ mouse livers (Figures 4B and S1A). The expression of *Hdac1* encoding histone acetylase, and SET domain bifurcated 1 (*Setdb1*), suppressor of variegation three to nine homolog 1 and 2 (*Suv39h1/2*) mRNA encoding histone H3 and lysine 9-specific methyltransferase, showed almost no change in Wy14,643-treated *Ppara*$^{+/+}$ mouse livers (Figure 4B). These results indicate that gene repression by UHRF1 depends on UHRF1 expression levels rather than DNMT1, HDAC1 or H3K9me3 expression levels.

UHRF1 was reported to localize to chromatin via binding to H3K9me3 (Karagianni et al., 2008; Kim et al., 2018). Therefore, RNA-seq data from livers of agonist-treated mice and H3K9me3 ChIP-seq data obtained from NCBI GEO Accession Number (GSE128073) were used to analyze the expression pattern of genes on chromosome (Chr) eight where *Cdh1* is located. Strong H3K9me3 ChIP-seq peaks were sandwiched between weak peaks, and were located within the 5′ upstream region of *Cdh1*, *Cdh3,* and sphingomyelin phosphodiesterase 3 (*Smpd3*) (Figure 4C). In addition, H3K9me3 ChIP-seq peaks were observed 5′ upstream of the microRNA let7c-1 (*Mirlet7c-1*) and its host gene*Mir99a* and the Mirlet7c-1 host gene (*Mir99ahg*) gene that are repressed by activated PPARA as shown in a previous study (Shah et al., 2007; Yagai et al., 2021) (Figure S2A). These genes are significantly down-regulated in response to PPARA agonist treatment (Figures 4D, S2B, and S3A).

To analyze protein expression and enzyme activity of methyltransferase complex, ChIP-qPCR, western blot and methyl-DNA immunoprecipitation analyses were performed. Enrichment of UHRF1, DNMT1, and HDAC1 in the promoter region of *Cdh1* was increased by PPARA activation, but the enrichment of H3K9me3 and SETDB1 was not changed (Figure 4E). Western blot results showed that only UHRF1expression was induced by PPARA activation (Figures 2C and 2D), but the expression of DNMT1, HDAC1, H3K9me3, and SETDB1 (Figures S4A and S4B) were not changed. In addition, 5-methylcytosine (5-mC) enrichment in the *Cdh1* promoter was induced in Wy14,643-treated *Ppara*$^{+/+}$ mouse livers, but not changed in Wy14,643-treated *Ppara*$^{-/-}$ mouse livers (Figure 4F). Taken together, these data suggest that UHRF1 induced by the activation of PPARA binds to H3K9me3 and recruits DNMT1 to enhance methylation of the *Cdh1* promoter.

Knockdown of E2F8 or UHRF1 reverses the repression of CDH1 by activated PPARA

To confirm that the PPARA-E2F8-UHRF1 axis regulates CDH1 expression, the signal transduction pathway was analyzed using E2F8 and UHRF1 knockdown livers. To knockdown E2F8 and UHRF1 in mouse liver, short hairpin RNA (shRNA)-expressing adeno-associated virus (AAV) was used. The knockdown efficiency of E2F8 and UHRF1 by AAV expressing *E2f8*-shRNA (shE2f8) and *Uhrf1*-shRNA (shUhrf1) was confirmed at the mRNA and protein level. In Wy14,643-treated mouse livers, E2F8 and UHRF1 expression was strongly repressed (more than 50%) by shE2f8 and shUhrf1, respectively (Figures 5A, 5B, 5E and 5F). In addition, E2F8 or UHRF1 knockdown reversed the downregulation of *Cdh1*, *Cdh3*, *Smpd3*, *Mir99ahg*, and *Mirlet7c-1* mRNA and CDH1 protein by Wy14,643 treatment (Figures 5A–5C, 5E–5G, S2C, and S3B). E2F8 or UHRF1 knockdown had little effect on *Dnmt1* and *Hdac1* mRNA expression (Figure S3B).

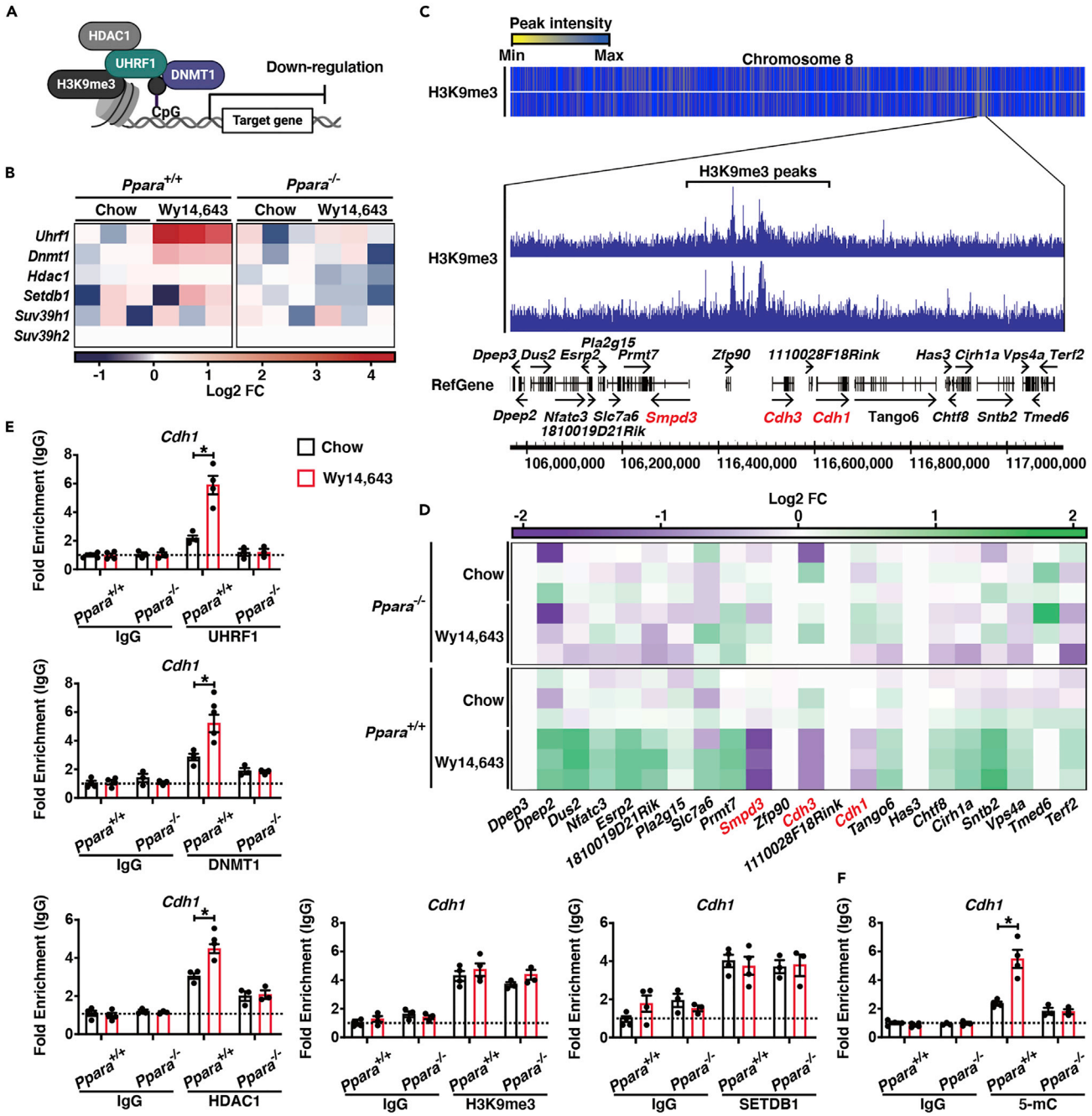

Figure 4. PPARA activation causes methylation of the *Cdh1* promoter marked on H3K9me3 in a UHRF1-dependent manner

(A) Model of gene repression by UHRF1.

(B) Heatmap of UHRF1-related gene expression provided from RNA-seq analyses in Wy14,643-treated *Ppara*$^{+/+}$ and *Ppara*$^{-/-}$ mouse livers. Mice fed either control chow diet or a diet containing 0.1% Wy14,643 for 48 h. n = 10–15 mice per group. Color key, Log2 fold-change (FC).

(C) H3K9me3 ChIP-seq reads peaks in 5′ upstream region of *Cdh1* in mouse livers.

(D) Heatmap of gene expression in the H3K9me3 binding peak provided from RNA-seq analyses in Wy14,643-treated *Ppara*$^{+/+}$ and *Ppara*$^{-/-}$ livers. Mice fed either a control chow diet or a diet containing 0.1% Wy14,643 for 48 h. n = 10–15 mice per group.

(E and F) UHRF1, DNMT1, HDAC1, H3K9me3, or SETDB1 ChIP-qPCR (E) or methyl-DNA immunoprecipitation analysis (F) assessed *Cdh1* promoter in liver samples from *Ppara*$^{+/+}$ and *Ppara*$^{-/-}$ mice treated with Wy14,643. Mice fed either control chow diet or a diet containing 0.1% Wy14,643 for 48 h. n = 3–4 mice per group. Significant differences from normal chow diet-treated each genotype mouse livers: *$p < 0.05$.

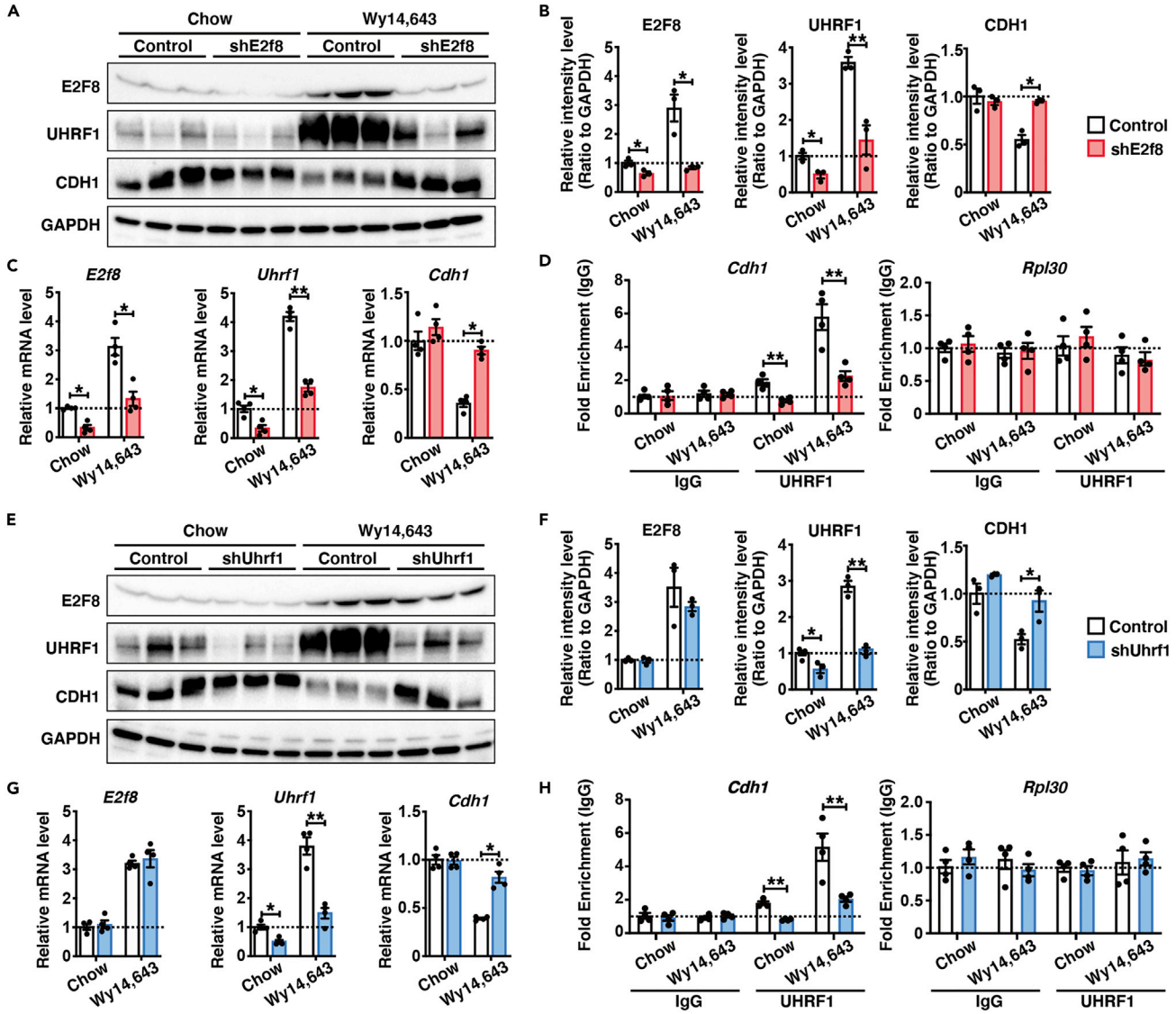

Figure 5. Repression of CDH1 expression by ligand-activated PPARA is reversed by the knockdown of E2F8 or UHRF1

Mice were fed either control chow diet or a diet containing 0.1% Wy14,643 for 48 h.

(A and B) Western blot analysis (A) and the quantification (B) of E2F8, UHRF1, and CDH1 proteins in AAV-shRNA-Control (Control) or AAV-shRNA-E2f8 (shE2f8)injected mice treated with Wy14,643. *n* = 3 mice per group.

(C) qRT-PCR analysis of *E2f8*, *Uhrf1*, and *Cdh1* mRNA in AAV-shRNA-Control (Control) or AAV-shRNA-E2f8 (shE2f8) injected mice treated with Wy14,643. *n* = 4 mice per group.

(D) UHRF1 ChIP-qPCR assessed *Cdh1* or *Rpl30* promoter region binding in liver samples from AAV-shRNA-Control (Control) or AAV-shRNA-E2f8 (shE2f8) injected mice treated with Wy14,643. *n* = 4 mice per group.

(E and F) Western blot analysis (E) and the quantification (F) of E2F8, UHRF1, and CDH1 proteins in AAV-shRNA-Control (Control) or AAV-shRNA-Uhrf1 (shUhrf1) injected mice treated with Wy14,643. *n* = 3 mice per group.

(G) qRT-PCR analysis of *E2f8*, *Uhrf1*, and *Cdh1* mRNA in AAV-shRNA-Control (Control)- or AAV-shRNA-Uhrf1 (shUhrf1)injected mice treated with Wy14,643. *n* = 4 mice per group.

(H) UHRF1 ChIP-qPCR assessed *Cdh1* or *Rpl30* promoter region binding in liver samples from AAV-shRNA-Control (Control) or AAV-shRNA-Uhrf1 (shUhrf1) injected mice treated with Wy14,643. *n* = 4 mice per group. Each data point represents the mean ± SEM Significant differences from shE2f8-or shUhrf1-treated mouse livers: $*p < 0.05$, $**p < 0.01$.

Next, ChIP-qPCR was used to confirm that UHRF1 binds to the promoter region of the *Cdh1*, *Cdh3*, *Smpd3*, and *Mir99ahg* genes; ribosomal protein L30 (Rpl30) was used as a negative control. The enrichment of UHRF1 binding to the *Cdh1*, *Cdh3*, *Smpd3*, and *Mir99ahg* promoter region was significantly amplified in

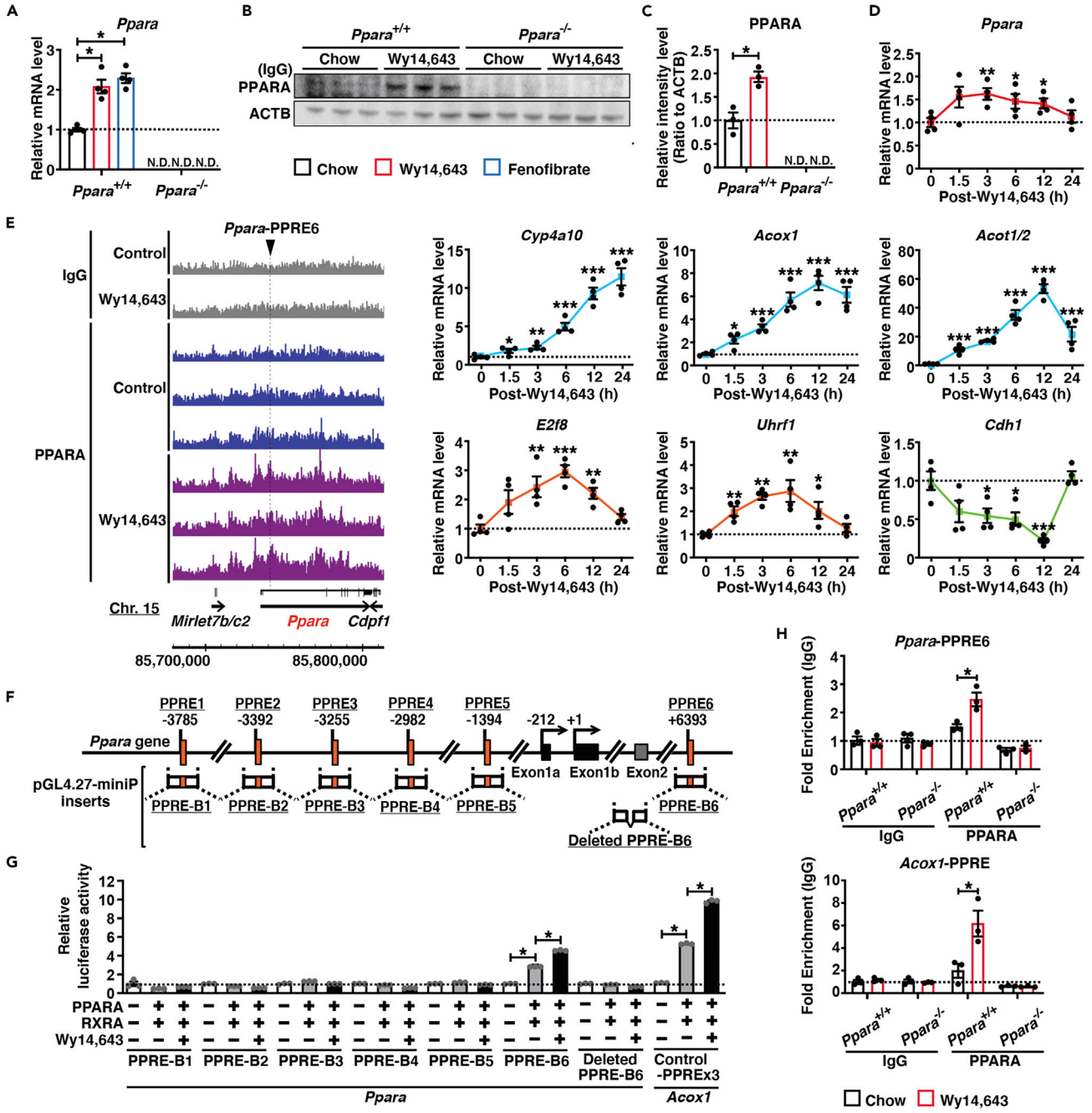

Figure 6. PPARA autoinduction accelerates the E2F8-UHRF1-CDH1 pathway

(A) qRT-PCR analysis of *Ppara* mRNA in Wy14,643- or fenofibrate-treated *Ppara*$^{+/+}$ and *Ppara*$^{-/-}$ mouse livers. *Ppara*$^{+/+}$ and *Ppara*$^{-/-}$ mice fed either control chow diet or a diet containing 0.1% Wy14,643 or 0.5% fenofibrate for 48 h. $n = 4$ mice per group. Significant differences from normal chow diet-treated each genotype mouse livers: $^{*}p < 0.001$.

(B and C) Western blot analysis (B) and the quantification (C) of PPARA protein in Wy14,643-treated *Ppara*$^{+/+}$ and *Ppara*$^{-/-}$ mouse livers. *Ppara*$^{+/+}$ and *Ppara*$^{-/-}$ mice fed either a control diet or a diet containing 0.1% Wy14,643 for 48 h. $n = 3$ mice per group. Significant differences from normal chow diet-treated each genotype mouse livers: $^{*}p < 0.01$.

(D) qRT-PCR analysis of *Ppara*, *Cyp4a10*, *Acox1*, *Acot1/2*, *E2f8*, *Uhrf1*, and *Cdh1* mRNAs in livers of *Ppara*$^{+/+}$ mice treated by gavage with Wy14,643 (50 mg/kg). Livers were collected at $t = 0$, 1.5, 3, 6, 12, and 24 h. $n = 4$ mice per group. Significant differences from Wy14,643-treated mouse livers (0 h): $^{*}p < 0.05$, $^{**}p < 0.01$, $^{***}p < 0.001$.

(E) PPARA ChIP-seq reads peaks in the *Ppara* and *Acox1* genes from Wy14,643-treated mouse livers. Mice were treated with Wy14,643 (50 mg/12 h/kg for 24 h) or vehicle by oral gavage and administered either a normal diet or a 0.1% Wy14,643-chow diet for 24 h. $n = 3$ mice per group.

Figure 6. *Continued*

(F) Schematic representation of the positions of the putative five PPRE sequences contained in the *Ppara* gene. Reporter gene construct inserts are shown.

(G) Luciferase reporter gene assay using the PPREs of the *Ppara* gene and its deleted-PPRE6 mutant, and *Acox1*-PPRE repeat. $n = 3$ per group. Significant differences from cells without PPARA/RXRA expression plasmid or without Wy14,643: $^{*}p < 0.001$.

(H) PPARA ChIP-qPCR assessed *Ppara*-PPRE6 or *Acox1*-PPRE binding in liver samples from $Ppara^{+/+}$ and $Ppara^{-/-}$ mice treated with Wy14,643. Mice fed either a control chow diet or a diet containing 0.1% Wy14,643 for 48 h. $n = 3$ mice per group. Significant differences from Wy14,643-treated $Ppara^{+/+}$ mouse livers: $^{*}p < 0.05$. Each data point represents the mean ± SEM.

control mouse livers by Wy14,643 treatment (Figures 5D, 5H, S2D, and S3C). On the other hand, enrichment of UHRF1 binding in the *Cdh1*, *Cdh3*, *Smpd3*, and *Mir99ahg* promoter region was observed to be significantly reduced in shE2f8- or shUhrf1-treated mouse liver compared with Control (Figures 5D, 5H, S2D, and S3C). These data suggest that the PPARA-E2F8-UHRF1 pathway negatively regulates CDH1 expression.

High expression through autoinduction of PPARA amplifies the E2F8-UHRF1-CDH1 pathway

To confirm that PPARA, E2F8, UHRF1, and CDH1 form a series of signal transduction pathways, the time course of gene expression after PPARA ligand treatment was analyzed. First, *Ppara* mRNA and PPARA protein levels in $Ppara^{+/+}$ and $Ppara^{-/-}$ livers were quantified. *Ppara* mRNA and PPARA protein expression in $Ppara^{+/+}$ mouse livers were induced by Wy14,643 or fenofibrate by approximately two-fold (Figures 6A–6C). The single dose of Wy14,643 was administered between 1 and 3 p.m. The peak *Ppara* mRNA levels were achieved only 3 h after a single dose of Wy14,643, whereas the expression of direct PPARA target gene mRNAs that are highly responsive to PPARA activation, *Cyp4a10*, *Acot1*, *Acot2* and *Acox1*, reach peak levels 12 or 24 h after Wy14,643 dosing (Figure 6D). *E2f8* and *Uhrf1* mRNA levels were most highly induced 6 h after a single dose of Wy14,643 (Figure 6D), whereas *Cdh1* expression was markedly repressed at 12 h after administration, following the induction of *E2f8* and *Uhrf1* (Figure 6D). Interestingly, *Mirlet7-c1* and *Mir99ahg* expressions were highly repressed from 1.5 to 12 h after a single dose of Wy14,643 (Figure S2E). These data suggest that PPARA autoinduction forms a positive feedback loop that accelerates the PPARA-E2F8-UHRF1-CDH1 signaling pathway.

To elucidate the mechanism of PPARA autoinduction by PPARA agonists, PPARA ChIP-seq was analyzed. PPARA ChIP-seq peaks, found within the genomic region containing the *Ppara* promoter and gene body, were found to contain six putative PPREs (Figures 6E, 6F and S1C). The PPRE found in the *PPARA* promoter region showed over 69% homology to the PPRE consensus sequence (Figure S1C). To identify functional PPREs, each *Ppara* PPRE (PPRE-B1 to -B6) was inserted into pGL4.27 containing the minimal promoter, and reporter gene expression assays performed (Figure 6F). A reporter construct containing a PPRE repeat from the rat *Acox1* gene (Control-PPREx3), which was employed in previous studies (Brocker et al., 2020), was used as a positive control to test for functional PPREs. Luciferase activity of *Ppara*-PPRE-B6 was induced by PPARA/RXRA by approximately three-fold, but not in *Ppara*-PPRE-B1 to B5 (Figure 6G). In addition, the induction of *Ppara*-PPRE-B6 luciferase activity by PPARA/RXRA was further induced by Wy14,643 treatment as in Control-PPREx3 (Figure 6G). The induction of *Ppara*-PPRE-B6 luciferase activity by PPARA/RXRA was completely abolished when transfection was carried out with *Ppara*-deleted PPRE-B6 constructs (Figure 6G).

Next, ChIP-qPCR using primers that specifically recognize the PPRE6 sequences, was performed to confirm that mouse PPARA specifically binds to PPRE6 located in intron two of the *Ppara* gene; $Ppara^{-/-}$ livers were used as a negative control to identify nonspecific binding. *Acox1* was used as a positive control for the PPARA binding enrichment. The enrichment of PPARA binding in *Ppara*-PPRE-B6 and *Acox1* was significantly amplified in $Ppara^{+/+}$ livers by Wy14,643 treatment (Figure 6H).

To examine whether PPARA/RXRA directly binds to *Ppara*-PPRE6, EMSA using *Ppara*-PPRE6 probes was performed. PPARA/RXRA directly bound to PPRE of the rat *Acox1* (control-PPRE) and *Ppara*-PPRE6 (Figure S1F). The binding of PPARA/RXRA to *Ppara*-PPRE6 was supershifted by anti-PPARA IgG (Figure S1F). Taken together, these data indicate that PPARA binds to a functional PPRE within its own promoter creating a positive feedback loop that increases PPARA expression and further potentiates the PPARA-E2F8-UHRF1-CDH1 pathway.

Forced expression of CDH1 suppresses hepatocyte hyperproliferation by activated PPARA

The loss of contact inhibition is a characteristic of cells lacking CDH1, and transfection of CDH1 into cells *in vivo* or *in vitro* was reported to reduce cell proliferation (Fujita et al., 2009; Gottardi et al., 2001; Navarro et al., 1991; St Croix et al., 1998; Yang et al., 2010). Therefore, the effect of forced expression of CDH1 on

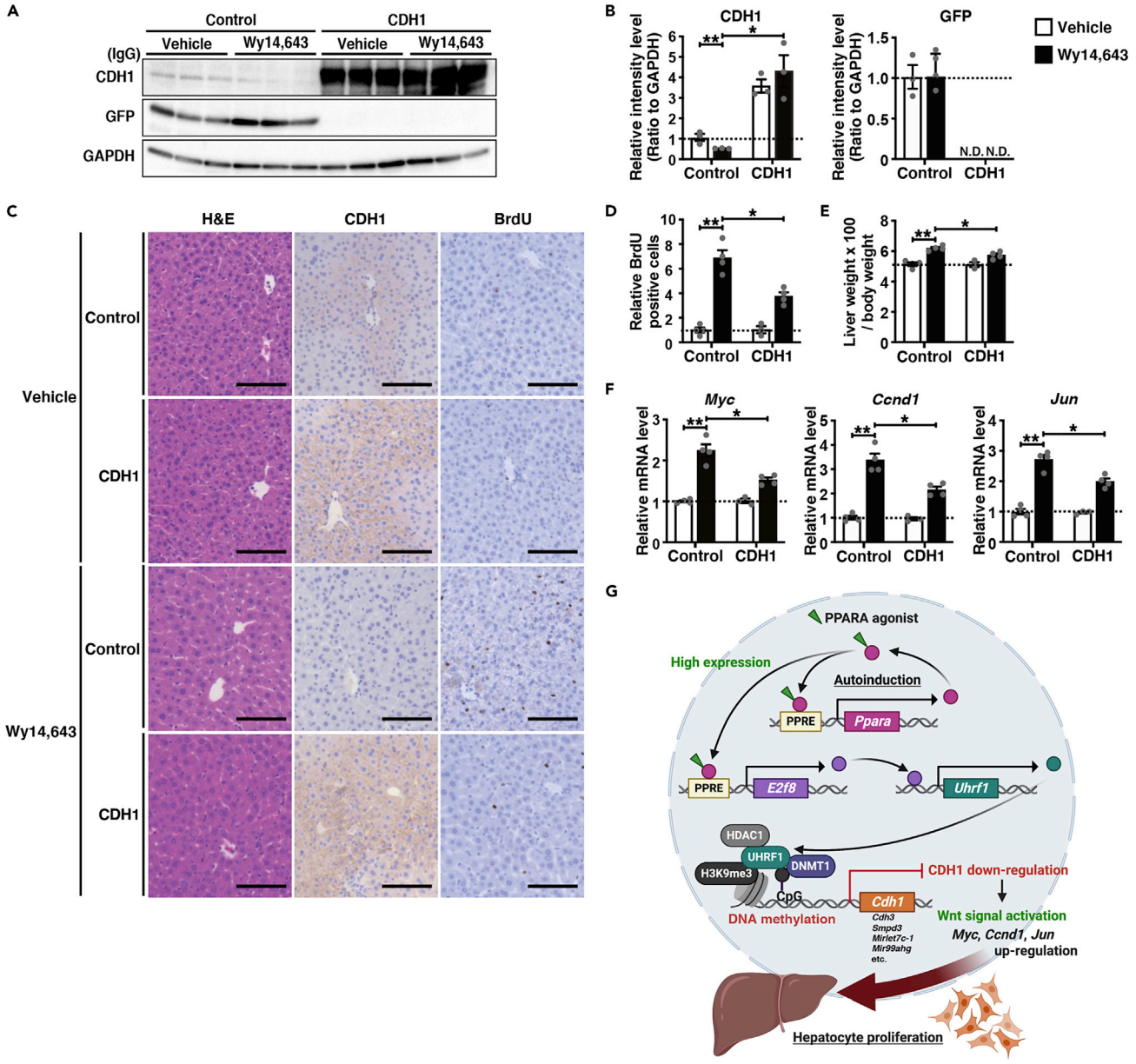

Figure 7. Hepatocyte hyperproliferation by ligand-activated PPARA is suppressed by the forced expression of CDH1

(A and B) Western blot analysis (A) and the quantification (B) of CDH1 and GFP proteins in pCMV3-GFP (Control) or pCMV3-CDH1 (CDH1) plasmids-injected mice treated with Vehicle or Wy14,643. n = 3 mice per group.

(C–E) H&E, CDH1-IHC, and BrdU-IHC staining (C), BrdU positive cells (D), and liver/body weight (E) in pCMV3-GFP (Control) or pCMV3-CDH1 (CDH1) plasmids-injected mice treated with Vehicle or Wy14,643. Scale bars represent 100 μm (200X).

(F) qRT-PCR analysis of *Myc*, *Ccnd1*, and *Jun* mRNAs in livers of pCMV3-GFP (Control) or pCMV3-CDH1 (CDH1) plasmids-injected mice treated with Vehicle or Wy14,643. Mice were treated with Wy14,643 (50 mg/12 h/kg for 36 h) or vehicle by oral gavage after injection each plasmid. Each data point represents the mean ± SEM n = 3–4 mice per group. Significant differences from normal chow treated Vehicle-Control-mouse livers or Wy14,643-Control-mouse livers: $*p < 0.05$, $**p < 0.01$.

(G) Schematic of the mechanism by which mouse PPARA controls hepatocyte proliferation through the E2F8-UHRF1-CDH1 axis.

hepatocyte proliferation by PPARA agonists was evaluated. Hepatic CDH1 expression and the tracking green fluorescent protein (GFP) expression as a negative control, were confirmed by western blotting 48 h after tail vein injection of the CDH1 or GFP expression vectors (Figures 7A and 7B). Wy14,643 treatment for mice was started 12 h after administration of the vector. Furthermore, no significant difference was

observed in plasma hepatic aspartate aminotransferase (AST) and alanine aminotransferase (ALT) between each group (Figure S5C).

Forced expression of CDH1 suppressed cell proliferation in Wy14,643-treated mouse livers confirming the role of CDH1 during PPARA-induced hepatocyte proliferation. Histological examination of liver sections by H&E (H&E) staining and immunohistochemistry (IHC) analysis showed characteristic hepatocyte swelling in response to Wy14,643 treatment in control mice (Figure 7C). CDH1 staining by IHC and immunofluorescence (IF) analysis was primarily at hepatocyte-hepatocyte junctions as previously reported (Maeda and Nakagawa, 2015; Nakagawa et al., 2014; Schneider et al., 2014), and was decreased significantly after Wy14,643 treatment when compared with controls (Figures 7C and S5D). Hepatic CDH1 expression was significantly increased in injected mice (Figures 7A–7C and S5D). Measurement of 5-bromo-2′-deoxyuridine (BrdU) uptake into cells is a useful index for determining the extent of cell proliferation. The number of BrdU-positive hepatocytes and the liver/body weight ratio were increased by Wy14,643 in control mice, but were significantly suppressed by CDH1 overexpression (Figures 7C–7E and S5D). In addition, both CDH1 and BrdU positive hepatocytes were observed predominantly around the large vein in the liver, and CDH1 overexpression reduced the number of BrdU-positive hepatocytes (Figures 7C and S5D). This result reveals that CDH1 and BrdU co-localize. Interestingly, some of the overexpressed CDH1 was localized to the same nuclei as BrdU in Wy14,643-treated hepatocytes (Figure S5D). Nuclear CDH1 has been observed in some proliferating cells (Zhao et al., 2019). Furthermore, the expressions of Wnt signaling target and proliferation marker genes induced by Wy14,643 treatment as such as *Myc*, *Ccnd1*, *Jun*, proliferating cell nuclear antigen (*Pcna*) and antigen identified by monoclonal antibody Ki 67 (*Mki67*) were significantly repressed by CDH1 overexpression (Figures 1F, 7F, S5A and S5B). These results suggest that the loss of CDH1 accelerates PPARA-induced hepatocyte proliferation through increased expression of the Wnt signaling target genes.

DISCUSSION

Recently, PPARA is not only be involved in lipid metabolism and inflammation (Brocker et al., 2020; Dubois et al., 2017; Wang et al., 2021), but also stimulates the proliferation of specific cell types such as mouse hepatocytes (Brocker et al., 2017), human glioma cells (Gao et al., 2018), zebrafish neuronal cells, and glial progenitor cells (Hsieh et al., 2018). However, the detailed mechanism by which PPARA stimulates cell proliferation remains unclear. This study revealed that PPARA activation in mice creates a feedforward loop where PPARA upregulates its own expression and causes hepatocyte proliferation via the E2F8-UHRF1-CDH1 axis. Agonist-induced upregulation of PPARA in mice was observed in several studies (Barbosa-da-Silva et al., 2015; Fischer et al., 2003; Fu et al., 2003; Kim et al., 2014; Kong et al., 2011; Li et al., 2018a), supporting the PPARA autoinduction mechanism described in the current work. In addition, this study found that the repression of CDH1 by PPARA was involved in stimulating cell proliferation via activation of Wnt signaling target genes such as *Myc*, *Ccnd1*, and *Jun*. These results suggest that alterations resulting in elevated expression of PPARA cause cell proliferation via the E2F8-UHRF1-CDH1-Wnt signaling axis.

of The present working model suggests that the autoinduction of PPARA in mice induces UHRF1 expression via E2F8, and the repression of CDH1 promotes hepatocyte proliferation by activation of Wnt signaling (Figure 7G). E2F8, UHRF1, CDH1, and the Wnt signaling target genes *Myc*, *Ccnd1*, and *Jun* located downstream of this PPARA signal, are all well-known genes involved in cell cycle regulation (Christensen et al., 2005; Shang et al., 2017; Tien et al., 2011). Cell cycle disorganization leads to uncontrolled cell proliferation (Golias et al., 2004). Therefore, the relationship revealed between E2F8, UHRF1, CDH1, and Wnt signaling target genes represents a potentially important signal transduction pathway that contributes to cell proliferation in mice.

This study revealed that *E2f8* and *Ppara* are novel PPARA target genes and explained the mechanism by which agonist binding to PPARA activates transcription of these genes. However, the involvement of cofactors in transcriptional regulation of *E2f8* and *Ppara* by PPARA remains unclear. Transcriptional activators of hepatic PPARA, PPAR binding protein (PBP), and mediator subunit 1 (MED1) were shown to be essential for PPARA agonist-dependent liver cancer/hepatocyte proliferation (Matsumoto et al., 2010). In addition, nuclear receptor corepressor (NCoR) and silencing mediator of retinoic acid and thyroid hormone receptor (SMRT) are the major co-repressors involved in regulation of liver metabolism by PPARA (Kang and Fan, 2020). Therefore, transcriptional activation of *E2f8* and *Ppara* by hepatic PPARA also likely involves the recruitment of PBP/MED1 and release of NCoR/SMRT.

During fasting, PPARA is activated by endogenous ligands such as N-oleoylethanolamine (OEA) and N-palmitoylethanolamine (PEA) (Fu et al., 2003; Izzo et al., 2010; Lo Verme et al., 2005), leading to induction of PPARA target gene expression (Kersten et al., 1999). E2F8 was reported to be induced in livers of fasted mice (Chen et al., 2019). The present study demonstrated that the *E2f8* gene is a direct hepatic PPARA target gene and that E2F8 is induced by Wy14,643 and fenofibrate. These results indicate that the *E2f8* gene is induced by PPARA synthetic ligands and endogenous ligands.

The *E2f8* transcripts, *E2f8-1a*, *E2f8-1b*, and *E2f8-1c*, are exon 1 splice variants, and these transcripts encode the amino acid sequence of the same protein (Maiti et al., 2005). In the current study, the expression of *E2f8-1a*, *E2f8-1b*, and *E2f8-1c* mRNA and total E2F8 protein was induced by PPARA activation. Therefore, all three variants of *E2f8* actively regulate the downstream UHRF1-CDH1 signal. Also, in this study, *E2f8* mRNA levels were not at different levels in *Ppara*$^{+/+}$ and *Ppara*$^{-/-}$ mouse livers. Because overexpression or knockout of E2F8 leads to cell cycle disruption (Deng et al., 2010; Kent et al., 2016), *E2f8* transcription in *Ppara*$^{-/-}$ mouse livers may be tightly regulated by unknown factors. On the other hand, E2F8 protein levels were decreased in *Ppara*$^{-/-}$ mouse livers. The lack of a correlation between *E2f8* mRNA and E2F8 protein levels may involve the E3 ubiquitin ligase complex for E2F8 such as anaphase promoting complex/cyclosome (APC/C) and SCF (Skp1-Cul1-F-box protein)$^{\text{Cyclin F}}$ (Cohen et al., 2013; Wasserman et al., 2020). Analysis of transcription factors controlling expression of *E2F8*, and the relationship between E2F8 and these E3 ubiquitin ligases in *Ppara*$^{-/-}$ mouse livers, warrant further study.

UHRF1 is a master regulator of the epigenome that allows crosstalk between DNA methylation and histone codes (Sidhu and Capalash, 2017). UHRF1 has various functional binding domains such as H3K9me3 (Karagianni et al., 2008; Rothbart et al., 2012), DNMT1 (Sharif et al., 2007), HDAC1 (Unoki et al., 2004) and methylated CpG (Unoki et al., 2004). Localization of UHRF1 is dependent on H3K9me3 (Karagianni et al., 2008; Kim et al., 2018) and recruiting DNMT1 and HDAC1 contributes to DNA methylation and heterochromatin formation (Bostick et al., 2007; Unoki et al., 2004). UHRF1 interacts with the maintenance DNA methyltransferase DNMT1 during the DNA replication phase and plays an essential role in inheritance of the DNA methylation pattern from parent cells to daughter cells (Li et al., 2018b; Nishiyama et al., 2013; Taylor et al., 2013). On the other hand, recruitment of UHRF1 to the gene promoter region contributes to the repression of gene expression (Babbio et al., 2012; Beck et al., 2018; Daskalos et al., 2011; Kim et al., 2009; Rajakumara et al., 2011). Overexpression of UHRF1 was reported to repress the expression of certain genes (Beck et al., 2018). In addition, it was shown that UHRF1 contributed to the silencing of *Cdh1* (Babbio et al., 2012). Accumulation of HDAC1 on the *Cdh1* promoter contributes to silencing of *Cdh1* via histone acetylation (Aghdassi et al., 2012; von Burstin et al., 2009). In this study, UHRF1 induced by PPARA activation recruited not only HDAC1 but also DNMT1 to the *Cdh1* promoter marked with H3K9me3, and repressed CDH1 expression via DNA methylation. These results support a mechanism by which PPARA can repress genes marked with H3K9me3 in a UHRF1-dependent manner.

Several mechanisms were proposed to explain how nuclear receptors cause ligand-dependent repression of target gene expression (Bartlett et al., 2019; Santos et al., 2011). PPARA represses gene expression by binding with specific transcription factors (Pawlak et al., 2015). However, repression of genes by PPARA activation cannot be explained by this mechanism. The current studies revealed that ligand-activated PPARA represses gene expression via methylation of the gene promoter marked with H3K9me3 by inducing the epigenetic regulator UHRF1 via E2F8. In addition, *Cdh1*, *Cdh3*, *Smpd3*, *Mir99ahg*, and *Mirlet7c-1* located in the gene region marked by H3K9me3 were all repressed. These results suggest that UHRF1 is able to repress multiple genes marked with H3K9me3 in a genome region-specific manner. This gene repression mechanism by ligand-activated PPARA may be widely applied to gene repression by other nuclear receptors.

Increased c-MYC expression is observed owing to chronic PPARA activation in mice (Peters et al., 2012). This study demonstrated that PPARA promoted *Myc* expression by activating Wnt signaling via the E2F8-UHRF1-CDH1 axis. Previous studies have shown that PPARA contributes to down-regulation of the *Mirlet7c-1* gene that targets and destabilizes *Myc* mRNA, which in turn causes increased MYC expression (Shah et al., 2007). From the combined analysis of PPARA ChIP-seq and H3K9me3 ChIP-seq, an H3K9me3 binding peak was found in the 5′ upstream region of the *Mirlet7c-1* gene, but a binding peak for PPARA was not observed. This indicates that PPARA does not directly down-regulate *Mirlet7c-1* expression but indirectly represses it through the E2F8-UHRF1 axis. In addition, RNA-seq data revealed that mouse PPARA activation represses more than 300 genes. Thus, the PPARA-E2F8-UHRF1 axis in rodents may contribute

to increased hepatocyte proliferation through global gene repression including targets such as *Mirlet7c-1* and *Cdh1*.

The repression of *Mirlet7c-1* by PPARA was not completely reversed in the livers of mice in which E2F8 and UHRF1 were knocked down. This result means that PPARA represses the expression of *Mirlet7c-1* through multiple mechanisms, not just the E2F8-UHRF1 pathway. The slight induction of epigenetic regulators other than UHRF1 by PPARA agonist supports this view. In addition, knockdown of E2F8 and UHRF1 in chow diet-treated mouse livers did not significantly induce *Cdh1*, *Cdh3*, *Smpd3*, *Mir99ahg*, and *Mirlet7c-1*. All of these genes are TSGs in the liver, and the loss of their expression is involved in the development and progression of HCC (Chirshev et al., 2019; Hu et al., 2016; Li et al., 2019; Revill et al., 2013; Zhong et al., 2018). Therefore, in chow diet-treated mouse livers, the expression of these genes is maintained at high levels and may not be sufficiently affected by induction owing to the loss of the PPARA-E2F8-UHRF1 pathway.

In summary, the present study demonstrated that PPARA represses CDH1 expression marked on H3K9me3 via the E2F8-UHRF1 axis and promotes cell proliferation via the CDH1-Wnt signaling axis. Furthermore, in this study, PPARA repressed many genes such as *Smpd3*, which encodes an important enzyme for ceramide production involved in lipid metabolism and inflammation (Chen and Cao, 2017; Wu et al., 2021). Therefore, the gene repression mechanism by PPARA found in this study may contribute not only to cell proliferation but also to various physiological functions of PPARA such as lipid metabolism and inflammation.

Limitations of the study

Whereas this study focused on specific genes involved in cell proliferation, such as *Cdh1*, the results suggested that the repression of gene expression of PPARA through hypermethylation of gene promoters marked by H3K9me3 may be a more generalized phenomenon. Thus, future studies should investigate a wider range of genes that are repressed by the PPARA-H3K9me3 axis by analyzing DNA and histone methylation patterns throughout the genome. As the studies in this report involved mouse models, it is not certain whether the results will fully translate to PPARA signaling in humans.

STAR★METHODS

Detailed methods are provided in the online version of this paper and include the following:

- KEY RESOURCES TABLE
- RESOURCE AVAILABILITY
  - Lead contact
  - Materials availability
  - Data and code availability
- EXPERIMENTAL MODEL AND SUBJECT DETAILS
  - Animals
- METHOD DETAILS
  - Cell culture
  - RNA-seq analysis
  - RT-qPCR
  - Western blot analysis
  - ChIP-seq and ChIP-qPCR
  - Methyl-DNA immunoprecipitation
  - Luciferase reporter assay
  - EMSA
  - AAV experiments
  - Biochemical analysis for serum ALT and AST
  - Hepatocyte proliferation
  - Database analysis
- QUANTIFICATION AND STATISTICAL ANALYSIS

SUPPLEMENTAL INFORMATION

Supplemental information can be found online at https://doi.org/10.1016/j.isci.2022.104196.

ACKNOWLEDGMENTS

We thank Linda G. Byrd and John R. Buckley for help with the animal protocols, management of the mouse colonies, and technical assistance with the mouse studies. This work was supported by the National Cancer Institute Intramural Research Program and by a grant from JSPS KAKENHI Grant Numbers (21K15424 and 17K08799) and Fukuoka University in Japan (D.A. and K.M.). S.T. and T.Y were supported in part by fellowship by the Japanese Society for the Promotion of Science. C.N.B. was supported in part by the Post-doctoral Research Associate Training (PRAT) program through the National Institute of General Medical Sciences, National Institutes of Health. D.K. was supported by a Korean Visiting Scientist Training Award. ST was supported by foundation of Georgetown University Medical Center. DNA sequencing was performed at the Center for Cancer Research (CCR) Genomics Core.

AUTHOR CONTRIBUTIONS

D.A., S.T., T.Y., D.K., C.N.B., and K.M. performed the research and analyzed the data. D.A., S.T., and F.J.G. designed the research. M.L. conducted review and editing. D.A., C.N.B., and F.J.G. wrote the manuscript. D.A., S.T., and F.J.G. supervised the research.

DECLARATION OF INTERESTS

The authors declare no competing interests.

Received: June 14, 2021
Revised: February 22, 2022
Accepted: March 31, 2022
Published: May 20, 2022

REFERENCES

Aghdassi, A., Sendler, M., Guenther, A., Mayerle, J., Behn, C.O., Heidecke, C.D., Friess, H., Büchler, M., Evert, M., Lerch, M.M., et al. (2012). Recruitment of histone deacetylases HDAC1 and HDAC2 by the transcriptional repressor ZEB1 downregulates E-cadherin expression in pancreatic cancer. Gut *61*, 439–448.

Aibara, D., Matsuo, K., Yamano, S., and Matsusue, K. (2019). Vaspin is a novel target gene of hepatic CCAAT-enhancer-binding protein. Gene *721*, 144113.

Aibara, D., Matsusue, K., Takiguchi, S., Gonzalez, F.J., and Yamano, S. (2018). Fat-specific protein 27 is a novel target gene of liver X receptor α. Mol. Cell Endocrinol. *474*, 48–56.

Alhosin, M., Omran, Z., Zamzami, M.A., Al-Malki, A.L., Choudhry, H., Mousli, M., and Bronner, C. (2016). Signalling pathways in UHRF1-dependent regulation of tumor suppressor genes in cancer. J. Exp. Clin. Cancer Res. *35*, 174.

Ashraf, W., Ibrahim, A., Alhosin, M., Zaayter, L., Ouararhni, K., Papin, C., Ahmad, T., Hamiche, A., Mély, Y., Bronner, C., et al. (2017). The epigenetic integrator UHRF1: on the road to become a universal biomarker for cancer. Oncotarget *8*, 51946–51962.

Babbio, F., Pistore, C., Curti, L., Castiglioni, I., Kunderfranco, P., Brino, L., Oudet, P., Seiler, R., Thalman, G.N., Roggero, E., et al. (2012). The SRA protein UHRF1 promotes epigenetic crosstalks and is involved in prostate cancer progression. Oncogene *31*, 4878–4887.

Barbosa-da-Silva, S., Souza-Mello, V., Magliano, D.C., Marinho Tde, S., Aguila, M.B., and Mandarim-de-Lacerda, C.A. (2015). Singular effects of PPAR agonists on nonalcoholic fatty liver disease of diet-induced obese mice. Life Sci. *127*, 73–81.

Bartlett, A.A., Lapp, H.E., and Hunter, R.G. (2019). Epigenetic mechanisms of the Glucocorticoid receptor. Trends Endocrinol. Metab. *30*, 807–818.

Beck, A., Trippel, F., Wagner, A., Joppien, S., Felle, M., Vokuhl, C., Schwarzmayr, T., Strom, T.M., von Schweinitz, D., Längst, G., et al. (2018). Overexpression of UHRF1 promotes silencing of tumor suppressor genes and predicts outcome in hepatoblastoma. Clin. Epigenetics *10*, 27.

Berger, J., and Moller, D.E. (2002). The mechanisms of action of PPARs. Annu. Rev. Med. *53*, 409–435.

Bostick, M., Kim, J.K., Estève, P.O., Clark, A., Pradhan, S., and Jacobsen, S.E. (2007). UHRF1 plays a role in maintaining DNA methylation in mammalian cells. Science *317*, 1760–1764.

Brocker, C.N., Kim, D., Melia, T., Karri, K., Velenosi, T.J., Takahashi, S., Aibara, D., Bonzo, J.A., Levi, M., Waxman, D.J., et al. (2020). Long non-coding RNA Gm15441 attenuates hepatic inflammasome activation in response to PPARA agonism and fasting. Nat. Commun. *11*, 5847.

Brocker, C.N., Yue, J., Kim, D., Qu, A., Bonzo, J.A., and Gonzalez, F.J. (2017). Hepatocyte-specific PPARA expression exclusively promotes agonist-induced cell proliferation without influence from nonparenchymal cells. Am. J. Physiol. Gastrointest. Liver Physiol. *312*, G283–G299.

Chen, Y., and Cao, Y. (2017). The sphingomyelin synthase family: proteins, diseases, and inhibitors. Biol. Chem. *398*, 1319–1325.

Chen, Y., Yu, D., Wang, L., and Du, S. (2019). Identification of E2F8 as a transcriptional regulator of Gluconeogenesis in primary mouse hepatocytes. Biochemistry (Mosc) *84*, 1529–1536.

Cheng, Y., He, C., Wang, M., Ma, X., Mo, F., Yang, S., Han, J., and Wei, X. (2019). Targeting epigenetic regulators for cancer therapy: mechanisms and advances in clinical trials. Signal Transduct. Target Ther. *4*, 62.

Chirshev, E., Oberg, K.C., Ioffe, Y.J., and Unternaehrer, J.J. (2019). Let-7 as biomarker, prognostic indicator, and therapy for precision medicine in cancer. Clin. Transl. Med. *8*, 24.

Christensen, J., Cloos, P., Toftegaard, U., Klinkenberg, D., Bracken, A.P., Trinh, E., Heeran, M., Di Stefano, L., and Helin, K. (2005). Characterization of E2F8, a novel E2F-like cell-cycle regulated repressor of E2F-activated transcription. Nucleic Acids Res. *33*, 5458–5470.

Cohen, M., Vecsler, M., Liberzon, A., Noach, M., Zlotorynski, E., and Tzur, A. (2013). Unbiased transcriptome signature of in vivo cell proliferation reveals pro- and antiproliferative gene networks. Cell Cycle *12*, 2992–3000.

Daskalos, A., Oleksiewicz, U., Filia, A., Nikolaidis, G., Xinarianos, G., Gosney, J.R., Malliri, A., Field, J.K., and Liloglou, T. (2011). UHRF1-mediated tumor suppressor gene inactivation in nonsmall cell lung cancer. Cancer *117*, 1027–1037.

Deng, Q., Wang, Q., Zong, W.Y., Zheng, D.L., Wen, Y.X., Wang, K.S., Teng, X.M., Zhang, X., Huang, J., and Han, Z.G. (2010). E2F8 contributes to human hepatocellular carcinoma via regulating cell proliferation. Cancer Res. *70*, 782–791.

Dongol, B., Shah, Y., Kim, I., Gonzalez, F.J., and Hunt, M.C. (2007). The acyl-CoA thioesterase I is regulated by PPARα and HNF4α via a distal response element in the promoter. J. Lipid Res. *48*, 1781–1791.

Dubois, V., Eeckhoute, J., Lefebvre, P., and Staels, B. (2017). Distinct but complementary contributions of PPAR isotypes to energy homeostasis. J. Clin. Invest. *127*, 1202–1214.

Fischer, M., You, M., Matsumoto, M., and Crabb, D.W. (2003). Peroxisome proliferator-activated receptor α (PPARα) agonist treatment reverses PPARα dysfunction and abnormalities in hepatic lipid metabolism in ethanol-fed mice. J. Biol. Chem. *278*, 27997–28004.

Fu, J., Gaetani, S., Oveisi, F., Lo Verme, J., Serrano, A., Rodríguez De Fonseca, F., Rosengarth, A., Luecke, H., Di Giacomo, B., Tarzia, G., et al. (2003). Oleylethanolamide regulates feeding and body weight through activation of the nuclear receptor PPAR-alpha. Nature *425*, 90–93.

Fujita, T., Liu, W., Doihara, H., and Wan, Y. (2009). An in vivo study of Cdh1/APC in breast cancer formation. Int. J. Cancer *125*, 826–836.

Gao, Y., Han, D., Sun, L., Huang, Q., Gai, G., Wu, Z., Meng, W., and Chen, X. (2018). PPARα regulates the proliferation of human glioma cells through miR-214 and E2F2. Biomed. Res. Int. *2018*, 3842753.

Golias, C.H., Charalabopoulos, A., and Charalabopoulos, K. (2004). Cell proliferation and cell cycle control: a mini review. Int. J. Clin. Pract. *58*, 1134–1141.

Gottardi, C.J., Wong, E., and Gumbiner, B.M. (2001). E-cadherin suppresses cellular transformation by inhibiting beta-catenin signaling in an adhesion-independent manner. J. Cell Biol. *153*, 1049–1060.

Heinz, S., Benner, C., Spann, N., Bertolino, E., Lin, Y.C., Laslo, P., Cheng, J.X., Murre, C., Singh, H., and Glass, C.K. (2010). Simple combinations of lineage-determining transcription factors prime cis-regulatory elements required for macrophage and B cell identities. Mol. Cell *38*, 576–589.

Hsieh, Y.C., Chiang, M.C., Huang, Y.C., Yeh, T.H., Shih, H.Y., Liu, H.F., Chen, H.Y., Wang, C.P., and Cheng, Y.C. (2018). Pparα deficiency inhibits the proliferation of neuronal and glial precursors in the zebrafish central nervous system. Dev. Dyn. *247*, 1264–1275.

Hu, Q.P., Kuang, J.Y., Yang, Q.K., Bian, X.W., and Yu, S.C. (2016). Beyond a tumor suppressor: soluble E-cadherin promotes the progression of cancer. Int. J. Cancer *138*, 2804–2812.

Hu, Y., Dai, M., Zheng, Y., Wu, J., Yu, B., Zhang, H., Kong, W., Wu, H., and Yu, X. (2018). Epigenetic suppression of E-cadherin expression by Snail2 during the metastasis of colorectal cancer. Clin. Epigenetics *10*, 154.

Inoue, K., and Fry, E.A. (2017). Haploinsufficient tumor suppressor genes. Adv. Med. Biol. *118*, 83–122.

Izzo, A.A., Piscitelli, F., Capasso, R., Marini, P., Cristino, L., Petrosino, S., and Di Marzo, V. (2010). Basal and fasting/refeeding-regulated tissue levels of endogenous PPAR-alpha ligands in Zucker rats. Obesity (Silver Spring) *18*, 55–62.

Kamata, S., Oyama, T., Saito, K., Honda, A., Yamamoto, Y., Suda, K., Ishikawa, R., Itoh, T., Watanabe, Y., Shibata, T., et al. (2020). PPARα ligand-binding domain structures with endogenous fatty acids and fibrates. iScience *23*, 101727.

Kang, Z., and Fan, R. (2020). PPARα and NCOR/SMRT corepressor network in liver metabolic regulation. FASEB J. *34*, 8796–8809.

Karagianni, P., Amazit, L., Qin, J., and Wong, J. (2008). ICBP90, a novel methyl K9 H3 binding protein linking protein ubiquitination with heterochromatin formation. Mol. Cell Biol. *28*, 705–717.

Kent, L.N., Rakijas, J.B., Pandit, S.K., Westendorp, B., Chen, H.Z., Huntington, J.T., Tang, X., Bae, S., Srivastava, A., Senapati, S., et al. (2016). E2f8 mediates tumor suppression in postnatal liver development. J. Clin. Invest. *126*, 2955–2969.

Kersten, S., Seydoux, J., Peters, J.M., Gonzalez, F.J., Desvergne, B., and Wahli, W. (1999). Peroxisome proliferator-activated receptor alpha mediates the adaptive response to fasting. J. Clin. Invest. *103*, 1489–1498.

Kim, D., Brocker, C.N., Takahashi, S., Yagai, T., Kim, T., Xie, G., Wang, H., Qu, A., and Gonzalez, F.J. (2019). Keratin 23 Is a peroxisome proliferator-activated receptor α-dependent, MYC-amplified oncogene that promotes hepatocyte proliferation. Hepatology *70*, 154–167.

Kim, J.H., Qu, A., Reddy, J.K., Gao, B., and Gonzalez, F.J. (2014). Hepatic oxidative stress activates the Gadd45b gene by way of degradation of the transcriptional repressor STAT3. Hepatology *59*, 695–704.

Kim, J.K., Estève, P.O., Jacobsen, S.E., and Pradhan, S. (2009). UHRF1 binds G9a and participates in p21 transcriptional regulation in mammalian cells. Nucleic Acids Res. *37*, 493–505.

Kim, K.Y., Tanaka, Y., Su, J., Cakir, B., Xiang, Y., Patterson, B., Ding, J., Jung, Y.W., Kim, J.H., Hysolli, E., et al. (2018). Uhrf1 regulates active transcriptional marks at bivalent domains in pluripotent stem cells through Setd1a. Nat. Commun. *9*, 2583.

Kong, L., Ren, W., Li, W., Zhao, S., Mi, H., Wang, R., Zhang, Y., Wu, W., Nan, Y., and Yu, J. (2011). Activation of peroxisome proliferator activated receptor α ameliorates ethanol induced steatohepatitis in mice. Lipids Health Dis. *10*, 246.

Kroetz, D.L., Yook, P., Costet, P., Bianchi, P., and Pineau, T. (1998). Peroxisome proliferator-activated receptor α controls the hepatic CYP4A induction adaptive response to starvation and diabetes. J. Biol. Chem. *273*, 31581–31589.

Leid, M., Kastner, P., Lyons, R., Nakshatri, H., Saunders, M., Zacharewski, T., Chen, J.Y., Staub, A., Garnier, J.M., Mader, S., et al. (1992). Purification, cloning, and RXR identity of the HeLa cell factor with which RAR or TR heterodimerizes to bind target sequences efficiently. Cell *68*, 377–395.

Li, G., Brocker, C.N., Xie, C., Yan, T., Noguchi, A., Krausz, K.W., Xiang, R., and Gonzalez, F.J. (2018a). Hepatic peroxisome proliferator-activated receptor α mediates the major metabolic effects of Wy-14643. J. Gastroenterol. Hepatol. *33*, 1138–1145.

Li, L., Yu, S., Wu, Q., Dou, N., Li, Y., and Gao, Y. (2019). KLF4-Mediated CDH3 upregulation suppresses human hepatoma cell growth and migration via GSK-3β signaling. Int. J. Biol. Sci. *15*, 953–961.

Li, T., Wang, L., Du, Y., Xie, S., Yang, X., Lian, F., Zhou, Z., and Qian, C. (2018b). Structural and mechanistic insights into UHRF1-mediated DNMT1 activation in the maintenance DNA methylation. Nucleic Acids Res. *46*, 3218–3231.

Lo Verme, J., Fu, J., Astarita, G., La Rana, G., Russo, R., Calignano, A., and Piomelli, D. (2005). The nuclear receptor peroxisome proliferator-activated receptor-alpha mediates the anti-inflammatory actions of palmitoylethanolamide. Mol. Pharmacol. *67*, 15–19.

Luo, Y., Xie, C., Brocker, C.N., Fan, J., Wu, X., Feng, L., Wang, Q., Zhao, J., Lu, D., Tandon, M., et al. (2019). Intestinal PPARα protects against colon carcinogenesis via regulation of methyltransferases DNMT1 and PRMT6. Gastroenterology *157*, 744–759.e744.

Maeda, S., and Nakagawa, H. (2015). Roles of E-cadherin in hepatocarcinogenesis. In Innovative Medicine: Basic Research and Development, K. Nakao, N. Minato, and S. Uemoto, eds. (Tokyo: Springer), pp. 71–77.

Magin-Lachmann, C., Kotzamanis, G., D'Aiuto, L., Cooke, H., Huxley, C., and Wagner, E. (2004). In vitro and in vivo delivery of intact BAC DNA – comparison of different methods. J Gene Med *6*, 195–209.

Maiti, B., Li, J., de Bruin, A., Gordon, F., Timmers, C., Opavsky, R., Patil, K., Tuttle, J., Cleghorn, W., and Leone, G. (2005). Cloning and characterization of mouse E2F8, a novel mammalian E2F family member capable of blocking cellular proliferation. J. Biol. Chem. *280*, 18211–18220.

Makia, N.L., and Goldstein, J.A. (2016). CYP2C8 is a novel target of peroxisome proliferator-activated receptor α in human liver. Mol. Pharmacol. *89*, 154–164.

Matsumoto, K., Huang, J., Viswakarma, N., Bai, L., Jia, Y., Zhu, Y.T., Yang, G., Borensztajn, J., Rao, M.S., Zhu, Y.J., et al. (2010). Transcription coactivator PBP/MED1-deficient hepatocytes are not susceptible to diethylnitrosamine-induced hepatocarcinogenesis in the mouse. Carcinogenesis *31*, 318–325.

Morimura, K., Cheung, C., Ward, J.M., Reddy, J.K., and Gonzalez, F.J. (2006). Differential susceptibility of mice humanized for peroxisome proliferator-activated receptor α to Wy-14,643-induced liver tumorigenesis. Carcinogenesis *27*, 1074–1080.

Nakagawa, H., Hikiba, Y., Hirata, Y., Font-Burgada, J., Sakamoto, K., Hayakawa, Y., Taniguchi, K., Umemura, A., Kinoshita, H., Sakitani, K., et al. (2014). Loss of liver E-cadherin induces sclerosing cholangitis and promotes

carcinogenesis. Proc. Natl. Acad. Sci. U S A. *111*, 1090–1095.

Navarro, P., Gómez, M., Pizarro, A., Gamallo, C., Quintanilla, M., and Cano, A. (1991). A role for the E-cadherin cell-cell adhesion molecule during tumor progression of mouse epidermal carcinogenesis. J. Cell Biol. *115*, 517–533.

Nishiyama, A., Yamaguchi, L., Sharif, J., Johmura, Y., Kawamura, T., Nakanishi, K., Shimamura, S., Arita, K., Kodama, T., Ishikawa, F., et al. (2013). Uhrf1-dependent H3K23 ubiquitylation couples maintenance DNA methylation and replication. Nature *502*, 249–253.

Park, S.A., Platt, J., Lee, J.W., López-Giráldez, F., Herbst, R.S., and Koo, J.S. (2015). E2F8 as a novel therapeutic target for lung cancer. J. Natl. Cancer Inst. *107*, djv151.

Pawlak, M., Lefebvre, P., and Staels, B. (2015). Molecular mechanism of PPARα action and its impact on lipid metabolism, inflammation and fibrosis in non-alcoholic fatty liver disease. J. Hepatol. *62*, 720–733.

Payne, S.R., and Kemp, C.J. (2005). Tumor suppressor genetics. Carcinogenesis *26*, 2031–2045.

Penvose, A., Keenan, J.L., Bray, D., Ramlall, V., and Siggers, T. (2019). Comprehensive study of nuclear receptor DNA binding provides a revised framework for understanding receptor specificity. Nat. Commun. *10*, 2514.

Peters, J.M., Shah, Y.M., and Gonzalez, F.J. (2012). The role of peroxisome proliferator-activated receptors in carcinogenesis and chemoprevention. Nat. Rev. Cancer *12*, 181–195.

Qu, A., Jiang, C., Cai, Y., Kim, J.H., Tanaka, N., Ward, J.M., Shah, Y.M., and Gonzalez, F.J. (2014). Role of Myc in hepatocellular proliferation and hepatocarcinogenesis. J. Hepatol. *60*, 331–338.

Rajakumara, E., Wang, Z., Ma, H., Hu, L., Chen, H., Lin, Y., Guo, R., Wu, F., Li, H., Lan, F., et al. (2011). PHD finger recognition of unmodified histone H3R2 links UHRF1 to regulation of euchromatic gene expression. Mol. Cell *43*, 275–284.

Rakhshandehroo, M., Knoch, B., Müller, M., and Kersten, S. (2010). Peroxisome proliferator-activated receptor α target genes. PPAR Res. *2010*, 612089.

Revill, K., Wang, T., Lachenmayer, A., Kojima, K., Harrington, A., Li, J., Hoshida, Y., Llovet, J.M., and Powers, S. (2013). Genome-wide methylation analysis and epigenetic unmasking identify tumor suppressor genes in hepatocellular carcinoma. Gastroenterology *145*, 1424–1435.

Rothbart, S.B., Krajewski, K., Nady, N., Tempel, W., Xue, S., Badeaux, A.I., Barsyte-Lovejoy, D., Martinez, J.Y., Bedford, M.T., Fuchs, S.M., et al. (2012). Association of UHRF1 with methylated H3K9 directs the maintenance of DNA methylation. Nat. Struct. Mol. Biol. *19*, 1155–1160.

Santos, G.M., Fairall, L., and Schwabe, J.W. (2011). Negative regulation by nuclear receptors: a plethora of mechanisms. Trends Endocrinol. Metab. *22*, 87–93.

Schneider, M.R., Hiltwein, F., Grill, J., Blum, H., Krebs, S., Klanner, A., Bauersachs, S., Bruns, C., Longerich, T., Horst, D., et al. (2014). Evidence for a role of E-cadherin in suppressing liver carcinogenesis in mice and men. Carcinogenesis *35*, 1855–1862.

Shah, Y.M., Morimura, K., Yang, Q., Tanabe, T., Takagi, M., and Gonzalez, F.J. (2007). Peroxisome proliferator-activated receptor α regulates a microRNA-mediated signaling cascade responsible for hepatocellular proliferation. Mol. Cell Biol. *27*, 4238–4247.

Shang, S., Hua, F., and Hu, Z.W. (2017). The regulation of β-catenin activity and function in cancer: therapeutic opportunities. Oncotarget *8*, 33972–33989.

Sharif, J., Muto, M., Takebayashi, S., Suetake, I., Iwamatsu, A., Endo, T.A., Shinga, J., Mizutani-Koseki, Y., Toyoda, T., Okamura, K., et al. (2007). The SRA protein Np95 mediates epigenetic inheritance by recruiting Dnmt1 to methylated DNA. Nature *450*, 908–912.

Sidhu, H., and Capalash, N. (2017). UHRF1: the key regulator of epigenetics and molecular target for cancer therapeutics. Tumour Biol. *39*, 1010428317692205.

St Croix, B., Sheehan, C., Rak, J.W., Flørenes, V.A., Slingerland, J.M., and Kerbel, R.S. (1998). E-Cadherin-dependent growth suppression is mediated by the cyclin-dependent kinase inhibitor p27(KIP1). J. Cell Biol. *142*, 557–571.

Taylor, E.M., Bonsu, N.M., Price, R.J., and Lindsay, H.D. (2013). Depletion of Uhrf1 inhibits chromosomal DNA replication in Xenopus egg extracts. Nucleic Acids Res. *41*, 7725–7737.

Tien, A.L., Senbanerjee, S., Kulkarni, A., Mudbhary, R., Goudreau, B., Ganesan, S., Sadler, K.C., and Ukomadu, C. (2011). UHRF1 depletion causes a G2/M arrest, activation of DNA damage response and apoptosis. Biochem. J. *435*, 175–185.

Unoki, M., Nishidate, T., and Nakamura, Y. (2004). ICBP90, an E2F-1 target, recruits HDAC1 and binds to methyl-CpG through its SRA domain. Oncogene *23*, 7601–7610.

Villarejo, A., Cortés-Cabrera, A., Molina-Ortíz, P., Portillo, F., and Cano, A. (2014). Differential role of Snail1 and Snail2 zinc fingers in E-cadherin repression and epithelial to mesenchymal transition. J. Biol. Chem. *289*, 930–941.

von Burstin, J., Eser, S., Paul, M.C., Seidler, B., Brandl, M., Messer, M., von Werder, A., Schmidt, A., Mages, J., Pagel, P., et al. (2009). E-cadherin regulates metastasis of pancreatic cancer in vivo and is suppressed by a SNAIL/HDAC1/HDAC2 repressor complex. Gastroenterology *137*, 361–371.

Wang, M., Yan, Y., Zhang, Z., Yao, X., Duan, X., Jiang, Z., An, J., Zheng, P., Han, Y., Wu, H., et al. (2021). Programmed PPAR-α downregulation induces inflammaging by suppressing fatty acid catabolism in monocytes. iScience *24*, 102766.

Wang, Y., Ngo, V.N., Marani, M., Yang, Y., Wright, G., Staudt, L.M., and Downward, J. (2010). Critical role for transcriptional repressor Snail2 in transformation by oncogenic RAS in colorectal carcinoma cells. Oncogene *29*, 4658–4670.

Wasserman, D., Nachum, S., Cohen, M., Enrico, T.P., Noach-Hirsh, M., Parasol, J., Zomer-Polak, S., Auerbach, N., Sheinberger-Chorni, E., Nevenzal, H., et al. (2020). Cell cycle oscillators underlying orderly proteolysis of E2F8. Mol. Biol. Cell *31*, 725–740.

Wu, Q., Sun, L., Hu, X., Wang, X., Xu, F., Chen, B., Liang, X., Xia, J., Wang, P., Aibara, D., et al. (2021). Suppressing the intestinal farnesoid X receptor/sphingomyelin phosphodiesterase 3 axis decreases atherosclerosis. J. Clin. Invest. *131*, e142865.

Yagai, T., Yan, T., Luo, Y., Takahashi, S., Aibara, D., Kim, D., Brocker, C.N., Levi, M., Motohashi, H., and Gonzalez, F.J. (2021). Feedback repression of PPARα signaling by Let-7 microRNA. Cell Rep. *36*, 109506.

Yang, L.J., Liu, Y.Q., Gu, B., Bian, X.C., Feng, H.L., Yang, Z.L., and Liu, Y.Y. (2010). Effect of forced E-cadherin expression on adhesion and proliferation of human breast carcinoma cells. Zhonghua Bing Li Xue Za Zhi *39*, 842–847.

Yu, H., Su, Y., Shin, J., Zhong, C., Guo, J.U., Weng, Y.L., Gao, F., Geschwind, D.H., Coppola, G., Ming, G.L., et al. (2015). Tet3 regulates synaptic transmission and homeostatic plasticity via DNA oxidation and repair. Nat. Neurosci. *18*, 836–843.

Zhao, Y., Yu, T., Zhang, N., Chen, J., Zhang, P., Li, S., Luo, L., Cui, Z., Qin, Y., and Liu, F. (2019). Nuclear E-cadherin acetylation promotes colorectal tumorigenesis via enhancing β-catenin activity. Mol. Cancer Res. *17*, 655–665.

Zhong, L., Kong, J.N., Dinkins, M.B., Leanhart, S., Zhu, Z., Spassieva, S.D., Qin, H., Lin, H.P., Elsherbini, A., Wang, R., et al. (2018). Increased liver tumor formation in neutral sphingomyelinase-2-deficient mice. J. Lipid Res. *59*, 795–804.

STAR★METHODS

KEY RESOURCES TABLE

REAGENT or RESOURCE	SOURCE	IDENTIFIER
Antibodies		
Rabbit polyclonal anti-PPARA	Abcam	Cat# ab24509; RRID: AB_448110
Rabbit monoclonal anti-RXRA	Cell Signaling Technology	Cat# 3085; RRID:AB_11140620
Rabbit polyclonal anti-E2F8	Abclonal	Cat# A1135; RRID: AB_2758519
Mouse monoclonal anti-UHRF1	Santa Cruz Biotechnology	Cat# sc-373750; RRID: AB_10947236
Rabbit monoclonal anti-UHRF1	Cell Signaling Technology	Cat# 12387; RRID: AB_2715501
Rabbit monoclonal anti-CDH1	Cell Signaling Technology	Cat# 3195; RRID: AB_2291471
Mouse monoclonal anti-ACTB	Santa Cruz Biotechnology	Cat# sc-47778; RRID: AB_626632
Rabbit polyclonal anti-GAPDH	MilliporeSigma	Cat# ABS16; RRID: AB_10806772
Rat monoclonal anti-BrdU	Abcam	Cat# ab6326; RRID: AB_305426
Mouse monoclonal anti-GFP	Medical & Biological Laboratories	Cat# M048-3; RRID: AB_591823
Mouse monoclonal anti-H3K9me3	Active Motif	Cat# 61013; RRID:AB_2687870
Rabbit polyclonal anti-SETDB1	Proteintech	Cat# 11231-1-AP, RRID: AB_2186069
Mouse monoclonal anti-DNMT1	Abcam	Cat# ab13537, RRID:AB_300438
Rabbit monoclonal anti-HDAC1	Abcam	Cat# ab7028, RRID:AB_305705
Mouse monoclonal anti-5-mC	Abcam	Cat# ab10805, RRID:AB_442823
Bacterial and virus strains		
AAV8-E2f8-shRNA	This paper	N/A
AAV8-Uhrf1-shRNA	This paper	N/A
Chemicals, peptides, and recombinant proteins		
Wy14,643	APExBIO Technology LLC	Cat# A4305
Fenofibrate	MilliporeSigma	Cat# F6020
Critical commercial assays		
SimpleChIP Plus Enzymatic Chromatin IP	Cell Signaling Technology	Cat# 9005
ALT assay kit	Catachem Inc	Cat# V164
AST assay kit	Catachem Inc	Cat# V154
Deposited data		
Raw and analyzed data (RNA-seq, PPARA ChIP-seq)	This paper	GSE154277
H3K9me3 ChIP-seq	-	GSE128073
Experimental models: Cell lines		
Mouse: Hepa-1c1c7 cells	ATCC	Cat# CRL-2026
Experimental models: Organisms/strains		
Mouse: C57BL/6	Charles River Laboratories	Strain Code: 027
Mouse: *Ppara* wild-type (*Ppara*$^{+/+}$), *Ppara*-null (*Ppara*$^{-/-}$)	Brocker et al., 2020	N/A
Oligonucleotides		
E2F8-PPREx3; see Figure S1	This paper	N/A
Oligo DNA sequences for RT-qPCR, ChIP-qPCR, Methyl-DNA immunoprecipitation, AAV shRNA construction, EMSA probes, and luciferase reporter construction; see Table S2	This paper	N/A
Recombinant DNA		
AAV-shRNA-Ctrl	Yu et al., 2015	N/A
pSG5-mouse PPARA	Addgene	Cat# 22751

(*Continued on next page*)

Continued

REAGENT or RESOURCE	SOURCE	IDENTIFIER
pSG5-mouse RXRA	Leid et al., 1992	N/A
pCMV3-mouse CDH1	Sino Biological	Cat# MG50671-CF
pCMV3-EGFP	Sino Biological	Cat# AG13105-CF
pGL4.27	Promega	Cat# E8451
phRL-TK	Promega	Cat# E6241
Software and algorithms		
GraphPad Prism	GraphPad software	https://www.graphpad.com/
JASPAR database	-	https://jaspar.genereg.net/
Integrated Genome Browser	-	https://www.bioviz.org/
Image J	-	https://imagej.nih.gov/ij/

RESOURCE AVAILABILITY

Lead contact

Further information and requests for resources and reagents should be directed to and will be fulfilled by the Lead Contact, Frank J. Gonzalez (gonzalef@mail.nih.gov).

Materials availability

Plasmids generated in this study are available from the lead contact without restriction.

Data and code availability

- RNA-seq and ChIP-seq data in this study have been deposited at GEO and publicly available at of the date of publication. Other raw data reported in this paper will be shared by the lead contact upon request.
- This paper does not report original code.
- Any additional information required to reanalyze the data reported in this paper is available from the lead contact upon request.

EXPERIMENTAL MODEL AND SUBJECT DETAILS

Animals

All animal studies and procedures were carried out in accordance with the Institute of Laboratory Animal Care international guidelines and approved by the National Cancer Institute Animal Care and Use Committee. *Ppara* wild-type ($Ppara^{+/+}$), *Ppara*-null ($Ppara^{-/-}$) and C57BL/6J male mice were used for this study. Mice were housed in a pathogen-free animal facility under a standard 12-h light/dark cycle (lights on at 7 AM) with free access to water and control chow diet (Bio-Serv, Frenchtown, NJ), 0.1% Wy14,643 (Bio-Serv) or 0.5% fenofibrate (Bio-Serv). For gavage administration, Wy14,643 (APExBIO Technology LLC, Houston, TX) was dissolved in 0.5% carboxymethyl cellulose (MilliporeSigma) and administered to mice at 50 mg/kg. All experiments were started with 6- to 9-week-old mice.

METHOD DETAILS

Cell culture

Hepa-1c1c7 (Hepa-1) mouse hepatoma cells (ATCC, Manassas, VA) were maintained at 37°C in a humidified atmosphere of 5% CO_2 in Dulbecco's Modified Eagle Medium containing 10% Fetal Bovine Serum (FBS) and 1% of penicillin/streptomycin mixture (Thermo-Fisher Scientific, Waltham, MA).

RNA-seq analysis

RNA sequencing (RNA-seq) was performed using livers of Wy14,643 or fenofibrate treated $Ppara^{+/+}$ and $Ppara^{-/-}$ mice. RNeasy Plus Mini Kit (Qiagen, Valencia, CA, USA) was used to extract total RNA from livers from six different treatment and control groups: $Ppara^{+/+}$ and $Ppara^{-/-}$ mice fed either control diet or a diet containing 0.1% Wy14,643 or 0.5% fenofibrate for 48 h. All mice were killed between 1 and 3 PM. The purity

and concentration of extracted RNA were measured by 4200 TapeStation system (Agilent). Library prep followed by RNA-seq was carried out by the National Cancer Institute Sequencing Facility. The RNA-seq library was prepared by use of the TruSeq Stranded mRNA Library Prep (Illumina). The library was analyzed by the Illumina HiSeq 2500 (Illumina). Sequencing files can be uploaded to NCBI GEO Accession Number GSE154275 as a part of the SuperSeries(GSE154277).

RT-qPCR

Total RNA was extracted from liver tissues using TRIzol reagent (Themo-Fisher Scientific) according to the manufacturer's instructions. A total of 1 μg total RNA was reverse transcribed into cDNA using qScript cDNA synthesis kit (Quantabio, Beverly, MA). The total RNA was treated with DNase I (Thermo-Fisher scientific) before reverse transcription. Reverse transcription quantitative real-time polymerase chain reaction (RT-qPCR) was performed using the PerfeCTa SYBR Green Supermix (Quanta Bio) in the QuanStudio 7 Flex System (Thermo-Fisher Scientific). Values were quantified with the comparative CT method, normalized to those of 18S ribosomal RNA (Rn18s) mRNA. Primer sequences are shown in Table S2.

Western blot analysis

Liver tissue was homogenized in radio immunoprecipitation assay lysis buffer (MilliporeSigma) containing the Halt Protease and Phosphatase Inhibitor Cocktail (Thermo-Fisher Scientific). The homogenates were centrifuged at 10,000 g for 10 min at 4 °C to obtain liver lysates, and protein concentrations measured with the Pierce BCA Protein Assay Kit (Thermo-Fisher Scientific). The liver lysates (20 μg protein) were dissolved in Laemmli sample buffer (Bio-Rad) with 5% 2-mercaptoethanol. The samples were loaded in 4%–15% Criterion TGX precast gels (Bio-Rad) followed by electrophoresis and transfer to PVDF membranes using a Trans-blot turbo transfer system (Bio-Rad). The protein transferred PVDF membrane was blocked in 5% nonfat milk followed by incubation with primary antibodies using anti-PPARA (Abcam; ab24509, 1:500), anti-E2F8 (Abclonal; A1135, 1:500), anti-CDH1 (Cell Signaling Technology; #3195, 1:1000), anti-RXRA (Cell Signaling Technology; #3085, 1:1000), anti-SETDB1 (Proteintech; 11231-1-AP, 1:1000) or anti-HDAC1 (Abcam; ab7028, 1:1000) rabbit antibodies, or anti-UHRF1 (Santa Cruz biotechnology; sc-373750, 1:500), anti-GFP (Medical & Biological Laboratories; M048-3, 1:1000), anti-H3K9me3 (Active Motif; 61,013, 1:1000) or anti-DNMT1 (Abcam; ab13537, 1:1000) mouse antibodies for overnight at 4°C. The β-actin (ACTB) or glyceraldehyde-3-phosphate dehydrogenase (GAPDH) band was obtained by reprobing the membranes with anti-ACTB (Santa Cruz biotechnology; sc-47778, 1:1000) mouse monoclonal antibody or GAPDH (MilliporeSigma; ABS16, 1:1000) rabbit polyclonal antibody used as a loading control. Goat anti-rabbit IgG-HRP (Santa Cruz biotechnology; sc-2357, 1:5000) or Goat anti-mouse IgG-HRP (Santa Cruz biotechnology; sc-2005, 1:5000) were used as the secondary antibodies. Each band intensity was quantified using ImageJ software (NIH, Bethesda MD), normalized by those of the loading control, and expressed as fold change relative to control wild-type mice.

ChIP-seq and ChIP-qPCR

Chromatin immunoprecipitation (ChIP) assays were performed using a SimpleChIP Plus Enzymatic Chromatin IP Kit-Magnetic Beads (Cell Signaling, #9005) according to the manufacturer's protocols. For PPARA ChIP-sequencing (ChIP-seq) analysis, mice were treated with Wy14,643 (50 mg/12 h/kg for 24 h) or vehicle (0.5% carboxymethylcellulose) by oral gavage, and administered either a normal diet or a 0.1% Wy14,643-chow diet for 24 h n = 3 mice per group. All mice were killed between 1 and 3 PM. For ChIP-qPCR analysis, mice were fed either a control chow diet or a diet containing 0.1% Wy14,643 for 48 h. n = 3-4 mice per group. All mice were killed between 1 and 3 PM. Control mouse livers or Wy14,643-treated mouse livers were treated with 1.5% formaldehyde (MilliporeSigma) for 15 min at room temperature. The isolated nuclei were digested with micrococcal nuclease for 25 min at 37°C and sonicated by Ultrasonic Processor (Cole-Parmer) to break the nuclear membrane on ice. Anti-PPARA IgG (Abcam; ab24509), anti-UHRF1 IgG (Cell Signaling; #12387), anti-DNMT1 IgG (Abcam; ab13537), anti-HDAC1 IgG (Abcam; ab7028), anti-H3K9me3 (Active Motif; 61013) and anti-SETDB1 (Proteintech; 11231-1-AP) was used to immunoprecipitate each protein binding DNA fragments. In a previous study, the specificity of PPARA antibody (Abcam; ab24509) was confirmed by western blot analysis using mouse liver nuclear extracts (Brocker et al., 2017). Normal Rabbit IgG (Cell Signaling, #2729) was used as a control IgG. The precipitated chromatin was digested with proteinase K for 2 h at 65 °C, and DNA was purified using a spin column. The purity and concentration of extracted DNA were measured by 4200 TapeStation system (Agilent Technologies). Library prep followed by PPARA ChIP-seq was operated by National Cancer Institute Sequencing Facility. The ChIP-seq library was prepared by NextSeq 500 Kit v1 (Illumina). The library

was analyzed by Illumina NextSeq 500 instrument (Illumina). Sequencing files are available under NCBI GEO Accession Number GSE154276 as a part of the SuperSeries(GSE154277). ChIP-seq data (wig files) were quantified and analyzed using the Integrated Genome Browser (IGB, pronounced Ig-Bee). ChIP-qPCR was performed using the PerfeCTa SYBR Green Supermix in the QuanStudio 7 Flex System. Values were quantified with the fold enrichment method. Primer sequences were shown in Table S2.

Methyl-DNA immunoprecipitation

Methyl DNA immunoprecipitation was performed as described previously (Luo et al., 2019). Genomic DNA of mouse livers was isolated using DNeasy Blood & Tissue Kit (QIAGEN) and was sheared by sonication to between 200 and 500 base pairs. The sonicated DNA was denatured at 95°C for 10 min. For each IP, 2 μg of denatured DNA was diluted in 500 mL IP buffer (0.05% Triton X-100 and 140 mM NaCl) with 2 μg anti-5-methylcytosine (5-mC) antibody (Abcam; ab10805) or Normal Rabbit IgG (Cell Signaling, #2729) and incubated overnight at 4°C. To collect the immune complex, 25 μL of protein G Dynabeads (Invitrogen) was added to each IP reaction mixture and incubated at 4°C for additional 4 h. Beads were immobilized using the magnetic rack and washed 3 times with an IP buffer. The immune complexes were eluted by incubation in a 500 μL proteinase K digestion buffer (0.5% SDS, 50 mM Tris-HCl, and 10 mM EDTA pH8.0) containing 5 μL/mL proteinase K solution (stock concentration, 20 mg/mL) at 50°C for 2 h. DNA was purified using MinElute Reaction Cleanup Kit (QIAGEN) and subjected to qPCR. Values were quantified with the fold enrichment method. Primer sequences were shown in Table S2.

Luciferase reporter assay

Luciferase reporter vectors were constructed by cloning the *Ppara*-PPRE-(B1-B6), *Ppara*-deleted PPRE-B6, *E2f8*-PPRE-(B1-B5), and *E2f8*-deleted PPRE-B4 sequences into an pGL4.27 vector (Promega) by HindIII and KpnI. These sequences used are listed in Table S2. The *E2f8*-PPREx3-B4 construct was prepared by inverse PCR (Figure S1C). Primer sequences are listed in Table S2. Hepa-1 cells were seeded at a density of 1.0×10^5 cells/well in 24-well plates at 12 h prior to transfection. Hepa-1 cells were transfected with plasmids using PEI Max transfection reagent (Polysciences) according to the manufacturer's instructions. Typically, each well contained 1 μL of 1 μg/μL PEI Max transfection reagent, 0.2 μg of pSG5-PPARA (Addgene; mouse/#22751) and RXRA (Leid et al., 1992) expression vectors, 0.1 μg of luciferase reporter vectors, and 0.01 μg of phRL/TK (Promega) as an internal control for transfection efficiency. After adding 50 μM Wy14,643 or vehicle (0.1% DMSO), cells were transfected for 6 h at 37°C in an atmosphere of 5% CO_2. The cells were then incubated for 42 h. During transfection and agonist or 0.1% DMSO treatment, Hepa-1 cells were cultured in DMEM containing 10% FBS and 1% of penicillin/streptomycin mixture. The luciferase assay was performed using the Dual-Luciferase Reporter Assay System (Promega, Madison, WI). Luciferase activity was measured using a Veritas Microplate Luminometer (Turner BioSystems).

EMSA

Electrophoretic mobility shift assay (EMSA) was performed as described previously (Aibara et al., 2019; Aibara et al., 2018). For the supershift assay, samples were incubated with 0.5 μg of anti-PPARA IgG (Abcam; ab24509) for 30 min after the binding reactions. The gels were exposed to an imaging plate (Fujifilm, Tokyo, Japan) and visualized using an FLA-7000 imaging analyzer (Fujifilm). Probe sequences for the EMSA assay were shown in Table S2.

AAV experiments

Adeno-associated virus (AAV)-short hairpin RNA (shRNA)-control (ctrl) was a gift from Hongjun Song (Yu et al., 2015). AAV gene delivery vectors were constructed by cloning the *E2f8* and *Uhrf1* guide sequence into an AAV-shRNA-Ctrl (Addgene, Watertown, MA) by BamHI and BglII. The shRNA sequences used are listed in Table S2. AAV2/8 viruses were produced, purified, and titrated according to the manufacturer's instructions (Addgene). Briefly, AAV2/8 viruses were generated by transfection of HEK293FT cells with the pAAV2 insert containing either shRNA control, shRNA-*E2f8*, or shRNA-*Uhrf1* and under control of the mouse U6 promoter, and flanked by serotype-2 inverted terminal repeats, pXR1 containing the rep and cap genes of AAV serotype-8, and pHelper encoding the adenovirus helper functions. Cell lysates were subjected to three rounds of freeze/thaw and then treated with 5 μL of benzonase (MilliporeSigma) for 45 min at 37 °C and clarified by centrifugation. Virus was purified by iodixanol gradient ultracentrifugation and titrated by qPCR. C57BL/6J mice were tail-vein injected with AAV-shRNA-Ctrl (as negative control) AAV-shRNA-*E2f8*, AAV-shRNA-*Uhrf1* at 1×10^{12} gc/mouse in 200 μL of saline. Before injection, mice

were exposed to heat lamp to dilate the tail vein and then placed in a restrainer permitting access to the tail vein. The tail was sterilized with 70% ethanol, and injection carried out in the lateral vein, using 27-gauge needles. Three weeks after infection, mice were treated with a control chow diet or 0.1% Wy14,643 for 48 h.

Biochemical analysis for serum ALT and AST

Serum samples were subjected to commercial serum alanine aminotransferase (ALT) and aspartate aminotransferase (AST) assay kit (Catachem, Bridgeport, CT) and monitored at 340 nm for 10 min with a microplate reader (BioAssay Systems, Harvard, CA).

Hepatocyte proliferation

C57BL/6J mice were tail-vein injected with pCMV3- CDH1 (Sino Biological, mouse/MG50671-CF,) or EGFP (Sino Biological, Aequorea Victoria/AG13105-CF) using PEI Max transfection reagent (PEI, Polysciences) according to a method modified from Magin-Lachmann et al. (2004). Briefly, plasmid/PEI complexes were prepared as follows (amounts are given per mouse). For pre-complexing with PEI, 40 μg plasmids were diluted with 100 μL saline and 80 μg PEI were diluted in 100 μL saline. The plasmid and PEI dilutions were mixed and incubated for least 30 min at room temperature. C57BL/6J mice were slowly injected in the tail vein with a total volume of 200 μL of plasmids/PEI complexes. Twelve h after injection, mice were treated with a total volume of 200 μL of Wy14,643 (50 mg/12 h/kg for 36 h) or vehicle (0.5% carboxymethylcellulose) by oral gavage and treated with a total volume of 200 μL of 1 mg 5-bromo-2′-deoxyuridine (BrdU, Abcam) by intraperitoneal injection once daily for 36 h. Forty-eight h after administration of plasmids/PEI complexes, mice were killed, and fresh liver tissue was immediately fixed in 10% phosphate-buffered formalin for 24 h. IHC and IF analysis for BrdU and CDH1, and hematoxylin and eosin (H&E) staining were performed by HistoServ, Inc. (Germantown, MD) using BrdU antibody (Abcam; ab6326) and CDH1 antibody (Cell Signaling; #3195).

Slide imaging was performed using a Keyence BZ-X700 series all-in-one microscope with both ×20 objectives, ×200 magnification, respectively. BrdU-positive cells were counted at least four sections per mouse and at 3-4 mouse livers per group by using Image J software (NIH, Bethesda MD). Relative BrdU-positive cells were showed BrdU-positive cells/total number of cells in area of 200 μm^2.

Database analysis

H3K9me3 ChIP-seq data was downloaded from NCBI GEO Accession Number (GSE128073). Integrated Genome Browser (IGB, pronounced Ig-Bee) were used to analyze the ChIP-seq data.

QUANTIFICATION AND STATISTICAL ANALYSIS

All results are expressed as means ± SEM. Significance was determined by t-test or one-way ANOVA with Bonferroni correction using Prism software (GraphPad Software, La Jolla, CA, USA). A p-value less than 0.05 was considered significant and statistical significance is indicated in the figure legends.